Ore Geology Reviews 150 (2022) 105109

Contents lists available at ScienceDirect

Ore Geology Reviews

journal homepage: www.elsevier.com/locate/oregeorev

Evolution of the Munali Intrusive Complex: Host to a carbonate-rich Ni-(Cu-PGE) sulfide deposit

Daryl E. Blanks [a,*,1], David A. Holwell [a,1], Stephen J. Barnes [b], Louise E. Schoneveld [b], Adrian J. Boyce [c], Laston Mbiri [d]

[a] Centre for Sustainable Resource Extraction, University of Leicester, University Road, Leicester LE1 7RH, UK
[b] CSIRO Mineral Resources, 26 Dick Perry Ave., Kensington, Western Australia 6151, Australia
[c] Scottish Universities Environmental Research Centre, Rankine Avenue, Scottish Enterprise Technology Park, East Kilbride G75 0QF, UK
[d] Mabiza Resources, Munali Nickel Mine, 10684 Kafue/Mazabuka Road, 50799 Lusaka, Zambia

A B S T R A C T

The Munali Intrusive Complex is hosted within supracrustal metasedimentary rocks located along a major structural lineament within the Zambezi Belt in southern Zambia. The complex comprises unmineralised gabbro surrounded by a marginal heterogeneous mafic–ultramafic breccia unit that is host to Ni-Fe sulfide. This marginal unit comprises a range of variably evolved brecciated mafic–ultramafic rocks that include gabbro, olivine-gabbro and dolerite, alongside younger, pegmatitic, apatite-magnetite-bearing clinopyroxenite, wehrlite and dunite. The magmatic evolution is most consistent with a model whereby early mafic rocks interact with hot, MgO- and volatile-rich melts along gabbro contacts, causing localised metasomatism of gabbro and pyroxenites, and progressively replacing pyroxene-rich rocks with olivine, forming pegmatitic 'replacive dunites'. Sulfide mineralisation is characterised by a carbonate-rich apatite-magnetite-bearing assemblage predominately present as lenses of semi-massive to massive sulfide ore. The complex is enveloped almost entirely within a unit of marble, yet C and O isotope signatures of carbonate at Munali have revealed a clear mantle signature for some of the carbonate associated with sulfide, alongside a more dominant, crustally derived component. The carbonate occurring alongside sulfide displays micro to macro textures signifying the presence of carbonate melts formed from anatectic melting of the country rocks. The presence of fracture sets that define coarse breccia clasts (>1 m) indicate that the host rock was significantly crystallised and brittly deformed prior to carbonate and sulfide melt infiltration. Both carbonate and sulfide melts appear to have independently utilised these pre-existing weaknesses producing a pseudobreccia, and accounting for the seemingly chaotic nature of the orebody. The indication of sulfide being a significantly later phase suggests that the sulfide did not form in situ and was mobilised from elsewhere to be subsequently emplaced late within the Munali system.

1. Introduction

A variety of magmatic Ni-Cu-PGE sulfide deposit styles are currently recognised, with differences largely defined by geodynamic and tectonic setting alongside host silicate compositions (e.g. Barnes et al., 2017a). Geodynamically, most sulfide-rich Ni-Cu-dominant deposits are located along or near to craton margins associated with deep lithospheric structures (Begg et al., 2010). To meet the projected demand for battery metals, small to medium sized mafic–ultramafic intrusions are an increasingly important exploration target for Ni-sulfide discoveries, as evidenced by targeted exploration in Western Australia with discoveries in the Fraser Belt including the Nova Deposit (Barnes et al., 2020a) and Rockford project (Legend, 2020), in addition to the Julimar Ni-Cu-PGE discovery, 70 km NE of Perth (Chalice-Mining, 2020). These intrusions, usually 100s of metres thick, are generally part of dyke-sill-conduit systems, forming zoned ultramafic–mafic intrusions, and are prospective as they signify dynamic systems with high magma fluxes and likelihood for crustal contamination from country rocks; these factors are important for generating immiscible sulfide liquid (Lesher, 2017; Barnes and Robertson, 2019). The morphology of intrusions, with structural traps at the base of sills, or choke points within conduits, control where large volumes of sulfide liquid can accumulate to form orebodies within a mafic–ultramafic complex (Barnes et al., 2016).

Sulfide matrix breccias are a common feature of Ni-sulfide orebodies and can be caused by many processes, including pure magmatic brecciation, sulfide liquid infiltration, and pre-, syn- and post-magmatic deformation, which are suggestive of dynamic emplacement and high mobility of sulfide liquid (Barnes et al., 2017b; Barnes et al., 2018; Barnes et al., 2020a; Járóka et al., 2019; Le Vaillant et al., 2020; Piña et al., 2006). The identification and classification of these brecciation processes and their relative timings during magmatic emplacement and sulfide mineralisation events are challenging, but have fundamental

* Corresponding author.
E-mail address: daryl.blanks@le.ac.uk (D.E. Blanks).
[1] ORCID ID: Blanks: 0000-0002-9695-4129; Holwell 0000-0002-1023-7357.

https://doi.org/10.1016/j.oregeorev.2022.105109
Received 30 September 2021; Received in revised form 6 September 2022; Accepted 18 September 2022
Available online 19 September 2022

importance in ore genesis and modification models. Furthermore, the location of many of these deposits along structural corridors at craton margins means they are often subject to additional deformation from subsequent tectonic reactivation.

The Munali Intrusive Complex (MIC) in Zambia appears to represent a small to medium-sized conduit-style intrusive complex (2.5 km × 500 m) host to the Munali Ni mine. Emplaced during the early Neoproterozoic, the complex lies along a major crustal fault system (Munali Fault), situated within the Zambezi Belt between the Congo and Kalahari Cratons (Fig. 1). The MIC comprises a composite mafic–ultramafic system, with an unmineralised gabbro core surrounded by sulfide-bearing marginal mafic–ultramafic rocks. However, the MIC displays many atypical characteristics, including apatite-magnetite- bearing Cr-poor ultramafic rocks and a carbonate-apatite rich sulfide orebody previously described as a multistage, enigmatic chaotic megabreccia with possible carbonatite affinities (Holwell et al., 2017). Despite this recent work, the origin of the intrusive phases, the abundant carbonate and, crucially, the emplacement controls of the complex, remain ambiguous.

In this study, we apply a multi-scale and multi-technique approach to interrogate the thus-far undefined syn- and post-emplacement magmatic structural controls on the MIC. This includes macro- and *meso*-scale mapping and observations of underground faces of the Enterprise orebody in the Munali mine, and micro-scale textural mineralogy. We present the first C-O isotope and bulk rock geochemical studies to unravel the source and emplacement dynamics of the different intrusive phases and test the proposed carbonatite influence. We show that the MIC does not host a chaotic sulfide breccia, but the orebody has a number of fundamental magmatic and structural controls.

2. Regional setting

The MIC is located in the Southern Province of Zambia, 60 km south of Lusaka within the western Zambezi Belt (Fig. 1), situated between the Congo and Kalahari Cratons (Evans, 2011). The belt, trending WNW-ESE, represents a medium–high grade metamorphic structural zone subjected to significant episodic extensional and collisional tectonism since the Neoproterozoic, expressing parallels to the Lufilian Belt in the north of the country (Johnson et al., 2005; Katongo et al., 2004). The

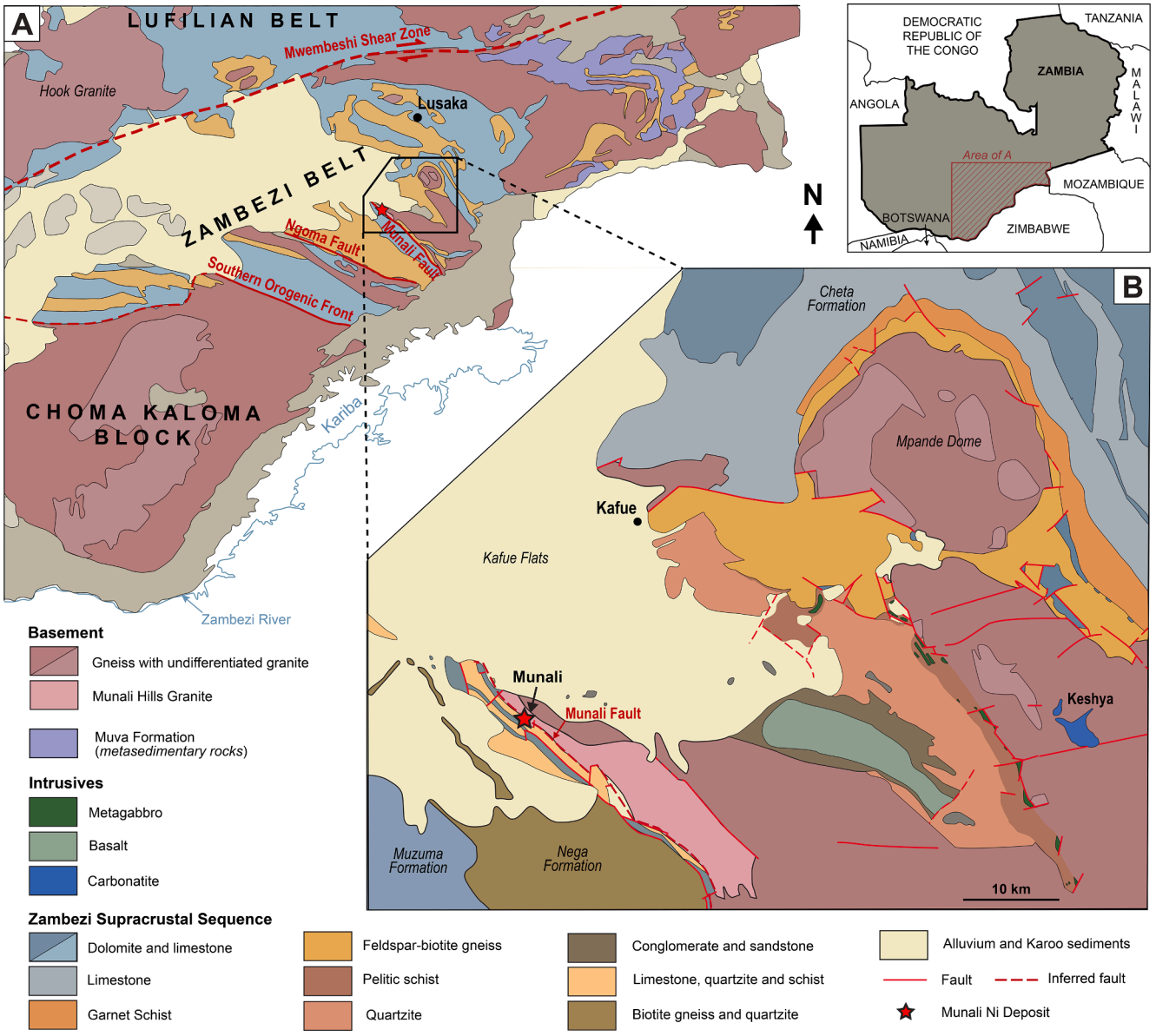

Fig. 1. A) Geological map of southern Zambia, showing locations of major fault zones of the Zambezi Belt; B) location of Munali within the Zambezi Supracrustal Sequence of the Zambezi Belt (after Smith, 1963).

Zambezi Belt extends from southern Zambia eastwards towards the western part of the Mozambique Belt, bounded to the south by the Choma-Kalomo Block and to the north by the Mwembeshi Shear Zone (a major sinistral tectonic boundary separating the Zambezi Belt from the Lufilian Belt) (Fig. 1A). Centrally the basement is comprised of the Mpande granitic gneiss (exposed around the Mpande Dome; Fig. 1B) emplaced at 1106 Ma (Hanson et al., 1988).

The geology and tectonic history of the Zambezi Belt is poorly constrained, the most significant preserved extensional event being related to the initial break-up of the supercontinent Rodinia resulting in continental thinning and extension, normal faulting, horst-graben development and deposition of siliciclastics and carbonates of the Zambezi Supracrustral Sequence (locally the Nega and Mulola Formation) from 870 to 820 Ma (Goscombe et al., 2020; De Waele et al., 2008). Emplacement of A-type granitic plutons (Ngoma Gneiss and Lusaka Granite) at ca. 820 Ma has been suggested to mark the final stages of the Zambezi rifting phase (Hanson et al., 1994).

At Munali, the tectonic history is less well defined and the local metasedimentary rocks have been previously assigned to the Mulola and Nega Formation of the Zambezi Supracrustal Sequence (Holwell et al., 2017; Johnson et al., 2007). These rocks are juxtaposed against basement rocks comprised of the Mpande Gneiss and the Munali Hills Granite (1090 ± 1.3 Ma; Katongo et al., 2004) that mark the Munali Hills ridge (Fig. 2). Subsequent regionally extensive rifting associated with the final break up of Rodinia continued until 725 Ma (Li et al., 2008; De Waele et al., 2008; Merdith et al., 2017), observed in the Lufilian and Damara Belts. However, all previous extensional tectonic phases have been overprinted and reactivated locally by at least two phases of subduction and collisional tectono-metamorphism from 640 Ma during the Pan-African Kuunga Orogeny (Goscombe et al., 2020), with peak metamorphism occurring at ca. 550–520 Ma, where the Zambezi Belt underwent NE-SW shortening and folding of the supracrustal sequence (Hanson et al., 1994).

Major shear zones mark the Zambezi Belt that includes the Munali Fault, Ngoma Fault and the Southern Orogenic Front along the northern margin of the Choma-Kalomo granitic block, which represents the orogenic front of the Zimbabwe Craton (Fig. 1). The Munali Fault signifies a major crustal lineament and preserves SW-directed thrusting that occurred within the Zambezi Belt during Pan-African orogenesis, whereby the Munali Hills granitic basement, Kafue Rhyolite and amphibolite-facies kyanite-scapolite metasedimentary rocks to the north of the fault having been juxtaposed against greenschist-facies andalusite-bearing Zambezi metasedimentary rocks to the south (Fig. 2A). The Munali Fault has been utilised by a range of mafic–ultramafic intrusions with many pod-like gabbroic and pyroxenite bodies, in addition to numerous magnetic anomalies, mostly located along the southern margin of the fault, which includes mafic–ultramafic intrusions of the MIC. To date, the MIC appears to represent the only intrusion locally discovered with significant magmatic Ni sulfide.

3. Munali Intrusive Complex

The MIC is an elongated, zoned complex, comprising a range of mafic and ultramafic intrusions. It is present as a chonolith structure that appears to be conformable to the host metasedimentary sequence layering, which have all been tilted approximately 70° to the SW (Fig. 2B). This work aims to build upon the geological framework of Holwell et al. (2017) and Evans (2011) summarised below, who divided the MIC into two units: a central gabbro unit (CGU), and a marginal ultramafic–mafic breccia unit (MUBU). The gabbro that makes up the CGU is the thickest and most voluminous of the intrusions, present at the core of the complex and we refer to it here as the central gabbro. Although variably textured, it is compositionally homogenous and characteristically unmineralised, containing no primary Ni and Cu sulfide.

The marginal mafic–ultramafic intrusions of the MUBU envelop the central gabbro and vary in thickness, with the ultramafic lithologies thickest on the SW margin and completely absent in places along the northern margin (Fig. 2). The marginal intrusions comprise a suite of dolerite, gabbro (often poikilitic), olivine-gabbro and apatite-magnetite bearing wehrlite, pyroxenite and dunite. Here we refer to them by their rock names and distinguish the gabbro of the MUBU from those of the CGU by referring to them as the marginal gabbros. The apatite-rich ultramafic rocks were referred to as olivinite and phoscorite by Holwell et al. (2017), the latter implying a carbonatitic-affinity; however, as the origin of the rocks remain unclear, we refer to them descriptively as apatite-magnetite-bearing dunite and wehrlite. The ultramafic rocks are commonly brecciated and host the sulfide as a sulfide-matrix ore breccia. Dating of zircons by CA-ID-TIMS provide U-Pb crystallisation ages of 862.4 ± 0.84 Ma for the marginal gabbro and 857.9 ± 2.1 Ma for the wehrlite, signifying a dynamic emplacement with an earlier mafic and later ultramafic episodes, consistent with cross cutting relationships observed underground and in core (Holwell et al., 2017). The age of the intrusions and localisation as a conformable structure within a unit of limestone, now marble, bounded by schists (Fig. 2), supports the emplacement as a sill into intraplate rift sediments.

Sulfide is present as massive to semi-massive ore and as weak disseminations and veins, predominately comprised of pyrrhotite≫pentlandite > chalcopyrite and sporadic pyrite, associated with abundant carbonate, magnetite and apatite gangue phases (Blanks et al., 2022). Sulfide appears spatially associated with ultramafic rocks and is present discontinuously within the marginal units. The sulfide is localised within three distinct zones marking the Munali prospects (Fig. 2), listed in order of sulfide abundance as: Enterprise (site of the Munali Ni mine), Intrepid and Voyager (all situated along the SW margin). Defiant, along the NE margin, contains no appreciable ultramafic rocks and only very minor sulfide.

4. Methods

Whole rock samples were prepared for major and trace element analysis by grinding in a Retsch planetary mill using agate pots and grinding balls. Major and trace element data were obtained on fusion beads and pressed powder pellets, respectively, by X-ray fluorescence (XRF) analysis using a PANalytical Axios Advanced X-ray fluorescence spectrometer at the University of Leicester, UK. The PANalytical Axios runs a 4 kW Rhodium anode end window ceramic technology X-ray tube. Total loss on ignition (LOI) was measured on pre-dried powders after ignition at 950 °C in air for 1 h. Selected Instrumental conditions avoid significant line overlaps within the usual compositional range for geological materials. Stability of current generation X-ray Spectrometry systems is such that measurements are no longer ratioed to a monitor sample to minimise instrumental drift effects but selected suitable drift monitoring samples are analysed at the commencement of each analytical run. Calibrations for major and trace element analyses were set using 50 international rock reference material (e.g., BCR-1, BHVO-1, W-2) under the same conditions and regressing the measured count rates against the recommended concentrations principally from Govindaraju (1994), Imai et al. (1995, 1996, 1999) and values published on the GeoREM reference site, utilising the Philips based Fundamental parameters correction technique. Analyses of international reference material indicate that precision for the observed data range and over the period of analytical work was 1–5 % (RSD) or better for major and trace elements.

Thin-section scale mapping was carried out on conventional polished thin sections and polished rock blocks using a Bruker M4 Tornado™ desktop scanning X-ray fluorescence spectrometer (μ-XRF), with a 40 μm polychromatic beam generated from a Rh tube operating at 50 kV and 500nA, and signal collection using an Xflash™ silicon drift detector at CSIRO, Perth, Australia. Sections were scanned at 40 μm resolution using a dwell time of 10 ms per pixel, and processed initially using Bruker's proprietary Esprit™ software. Phase maps were generated using a clustering algorithm within CSIRO proprietary Chimage™

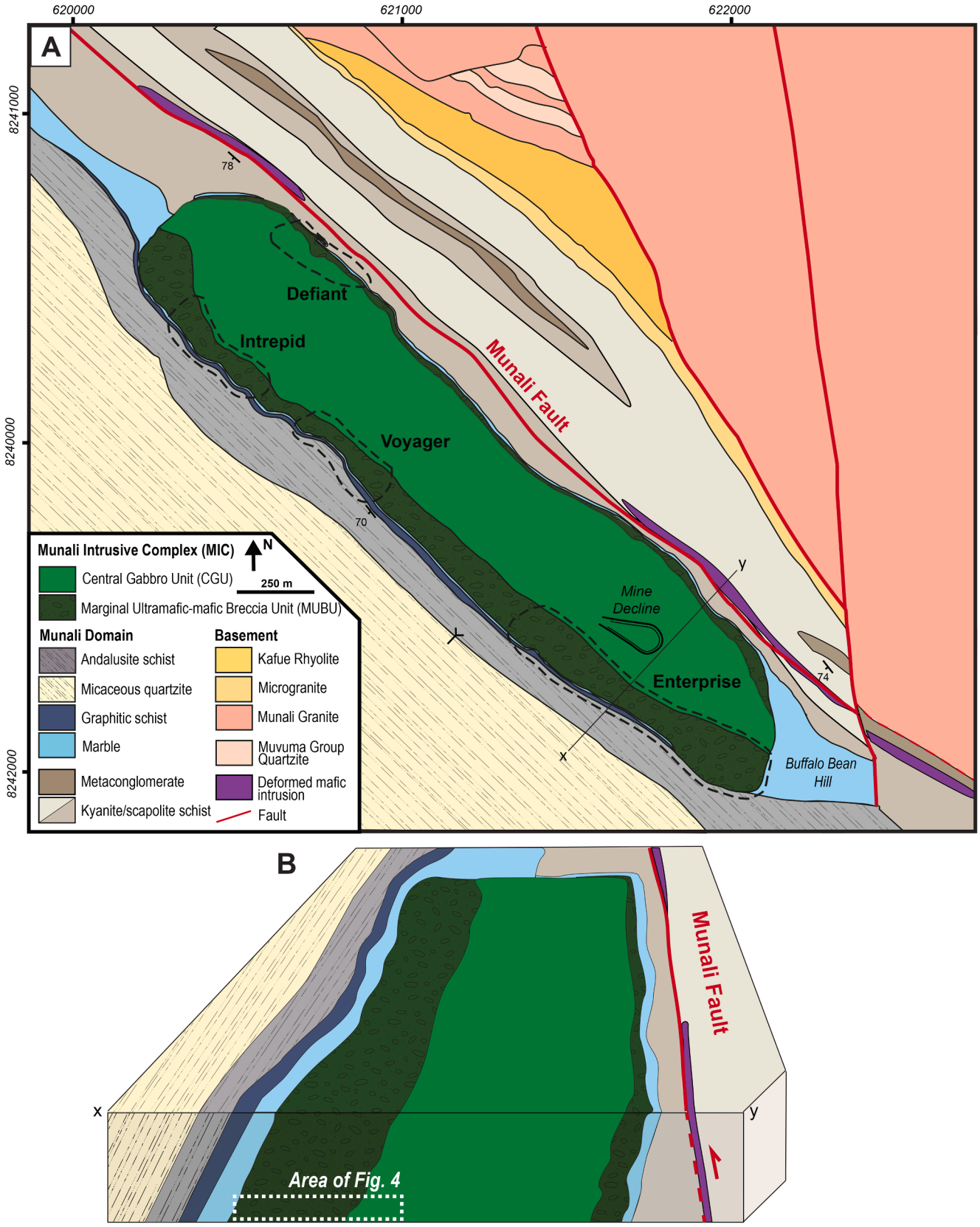

Fig. 2. A) Geological map of the Munali Intrusive Complex highlighting the marginal mafic–ultramafic units along the northern and southern margins, Munali Fault, local metasedimentary and basement rocks. B) Schematic cross-section of the Munali Intrusive Complex showing geometry and relationship to country rocks and association with the Munali Fault.

software (Wilson and MacRae, 2005).

Thorium, U and rare earth element (La, Ce, Pb, Pr, Nd, Sm, Hf, Ta, Eu, Gd, Tb, Dy, Ho, Er, Tm, Yb and Lu) concentrations were determined on 36 samples at the University of Leicester by a Thermo Scientific ICAP-Qc quadrupole ICP mass spectrometer. Samples were prepared using a standard HF-HNO_3 digestion. International standards and geochemical reference materials BCR-1 (basalt), AGV-1 (andesite) and JR-3 (rhyolite) were used to calibrate and evaluate the analytical data quality.

Trace element concentration in apatite were determined using laser-ablation inductively coupled plasma mass spectrometry (LA-ICP-MS) at CSIRO, Perth, Australia. Analysis was carried out with lines of a 50-μm-diameter circle traversing the sample at a rate of 5 μm/s at laser frequency of 9 Hz. Thirty seconds of background was collected at the start of each line analysis (>30 s). The following isotopes were measured in this study: ^{44}Ca, ^{55}Mn, ^{88}Sr, ^{89}Y, ^{139}La, ^{140}Ce, ^{141}Pr, ^{146}Nd, ^{147}Sm, ^{153}Eu, ^{157}Gd, ^{159}Tb, ^{163}Dy, ^{165}Ho, ^{166}Er, ^{169}Tm, ^{172}Yb and ^{175}Lu. Data was reduced using Iolite software (Paton et al., 2011). ^{44}Ca was used as internal standard for apatite minerals. The certified reference material G_BCR, G_NIST610 and G_NIST612 were used to check the accuracy and precision of the analysis during each analytical session where blocks of standards were measured at the beginning and end of the run, as well as between every ~ 10 unknown analyses and between different samples.

Carbonate-bearing samples from the MIC were collected from underground mine faces and drill core and country rock samples collected from drill core and outcrops up to 3 km away from the MIC for C and O isotopic analysis. Samples from Kovdor, Russia, and Phalaborwa, South Africa were taken from the collections at the University of Leicester as exemplars of phoscorite-carbonatite complexes. The C and O stable isotope composition of calcite, dolomite and magnesite were analysed at the Scottish Universities Environmental Research Centre (SUERC) on an Analytical Precision AP2003 mass spectrometer equipped with a separate acid injector system. Measured O isotope ratios are reported as per mil deviations relative to Vienna Standard Mean Ocean Water (VSMOW) and C isotopes relative to Vienna PeeDee Belemnite (VPDB) using conventional delta (δ) notation. Mean analytical reproducibility based on replicates of the SUERC laboratory standard NBS 18 (carbonatite from Fen, Norway) was around +/- 0.25 ‰ for both C and O.

5. Field relationships

5.1. Host rocks

The Munali Fault has been recognised as a major crustal lineament of the western Zambezi Belt, orientated NW-SE (Figs. 1 and 2), with granites and kyanite-scapolite schists to the north of the fault, and andalusite-bearing marbles and schists to the south, coincident with magnetic differences. However, our mapping has revealed that the fault is marked by the presence of previously unrecognised grey, highly deformed fine-grained, biotite-rich mafic intrusions exposed in three localities in close proximity to the northern margin of the Munali Complex (Fig. 2). Locally these intrusions and local sedimentary rocks dip 70 − 80° to the SW, are highly deformed and exhibit isoclinal folds that have locally developed into sheath folds (Fig. 3). The sense of compression during the deformation was interpreted from the axial plane within the sheath folded mafic rocks (Fig. 3A), striking 144°, and dipping 78° to the NE, determined to represent NE-SW vergence. The

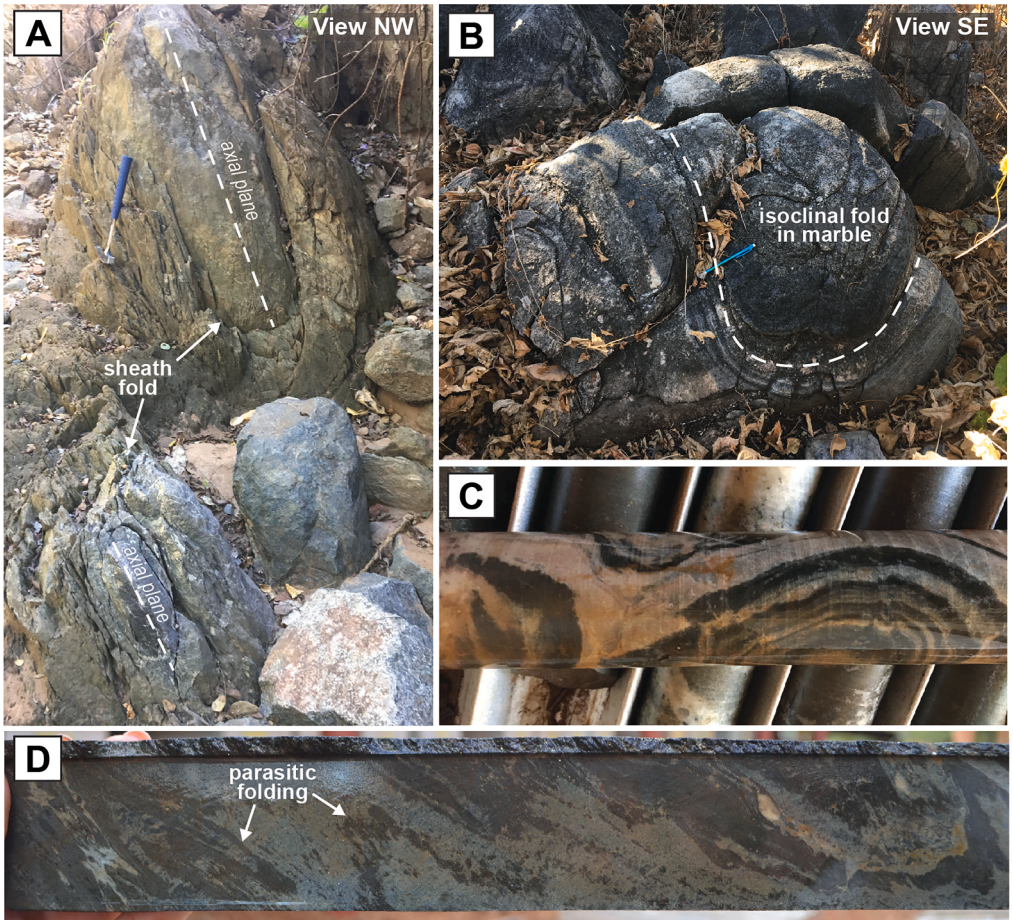

Fig. 3. Deformation of local sediments along the north-eastern margin of the Munali Intrusive Complex. A) Sheath folds in mafic rocks; B) sheath folds and isoclinal folding in marble at Buffalo Bean Hill to the south-west of the complex; C) strongly folded metasediments within drillcore at Defiant; D) sheared and folded rocks in drillcore of the Defiant prospect.

sense of simple shear is indicated by the long axis of the sheath folds that are subvertical in orientation (Fig. 3A).

The northern margin of the Munali Complex lies adjacent to the Munali Fault, and metasedimentary rocks are more deformed than the southern margin of the complex, with pervasive folding and minor faulting (Fig. 3C,D) and numerous marble lenses within gabbro. Notably ultramafic rocks are almost entirely absent and sulfide appears to be less abundant with only prospect, Defiant, identified to date (Fig. 2), where sulfide is present as sporadic semi-massive sulfide lenses in thicknesses of < 1 m associated with gabbro.

5.2. The Munali Intrusive Complex

The overall field relationships of the mafic–ultramafic rocks of the MIC are schematically represented in Fig. 4 as observed from mapping underground faces of the Munali Mine at Enterprise. Mapping has highlighted the nature of the orebody and the temporal and spatial relationship of the dynamic phases on both metre and centimetre scale.

5.2.1. Mafic rocks

Gabbro is the oldest and principal rock type of the complex occurring both in the centre as the sole lithology of the central gabbro and as part of the surrounding marginal ultramafic–mafic unit. The central gabbro is the thickest intrusive unit. It is texturally diverse with coarse pegmatitic, poikilitic and micro- gabbro comprising plagioclase (commonly altered to sericite and scapolite), and subhedral to anhedral clinopyroxene (altered to epidote and actinolite) with interstitial magnetite. Disseminated pyrite is the sole sulfide phase, and the central gabbro is considered barren of Ni-Cu mineralisation. However, late stage veins of carbonate ± (Ni-Cu-) sulfide are hosted throughout the central gabbro (Fig. 5), and are particularly focussed towards the contact with the principal massive sulfide orebody of the marginal unit.

The marginal gabbro resides towards the outer margins of the MIC, typically in contact with the country rock marble. No chilled margin is evident, instead, the contact is marked by a diffuse hybrid zone comprised of bleached marble and carbonate-rich 'hybrid' gabbro (Figs. 4 and 6A).

The marginal gabbro is the dominant intrusive component of the marginal mafic–ultramafic unit in the shallower levels of the Enterprise mine and is often locally brecciated and cut through by sulfide veins (Fig. 4). The marginal gabbro, although similar compositionally to the central gabbro, is commonly characterised by a distinct poikilitic texture with plagioclase crystals that are sometimes preferentially aligned, alongside clinopyroxene and magnetite (Fig. 6B-C). The gabbro contains rare sporadic disseminated pyrrhotite, pentlandite and chalcopyrite in addition to pyrite.

Previously unrecognised olivine-gabbro is a common rock type within the marginal units (Fig. 7). It is comprised of a similar mineralogy to the gabbro, but is intensely altered with the addition of serpentinised olivine and interstitial patches of pyrrhotite, pentlandite and chalcopyrite (Fig. 7F). The rock is generally medium-coarse grained, displays a variation of textures but typically comprises patchy elongated serpentinised olivine, with the rock itself commonly located towards the centre of the marginal units, spatially associated with the ultramafic rocks.

The intrusive complex is cross-cut by thin (<1 m) sub-vertical dolerite intrusions (Fig. 4) that are unmineralised with no associated sulfide, and petrologically comprise a fine-grained plagioclase groundmass with olivine and clinopyroxene phenocrysts. Dolerite is easily distinguished in underground mine faces due to being a homogenous dark black colour when viewed underground (Fig. 4B), in addition to being less deformed and brecciated than the ultramafic and mafic rocks of the marginal units, which led Holwell et al. (2017) to suggest that the dolerite was synchronous with sulfide emplacement.

5.2.2. Ultramafic rocks

Ultramafic rocks are a principal component of the marginal unit and are also observed to intrude the central gabbro. The ultramafic lithologies are all apatite-bearing and comprise pervasively altered dunite, with rare wehrlite and olivine-clinopyroxenite lenses. The ultramafic rocks are present in greater thicknesses in the deeper parts of the orebody at the Enterprise mine, along the base of the marginal units, in contact with the central gabbro (Fig. 4). The ultramafic rocks are ubiquitously coarse grained (>1 cm), containing varying proportions of magnetite (between 5 and 20 %) (Fig. 8). In addition, pink, white and rarer green apatite is present as coarse interstitial (>1 cm) crystals in all the ultramafic rocks, with up to 5 % modal abundance (Fig. 8B,C,F), alongside rare interstitial calcite (Fig. 8B,E). At the Enterprise mine and the Voyager prospect, (apatite-)magnetite-bearing dunite is the dominant ultramafic rock. Pyroxenes are rare, present exclusively as clinopyroxene within wehrlite and clinopyroxenite (Fig. 8E,F). These pyroxene-rich ultramafic rocks are present mainly in the western end of the south-western margin of the complex (Intrepid prospect), where dunite is absent. At Intrepid, the wehrlite and clinopyroxenite are spatially associated with marginal (olivine)-gabbros. Here the marginal gabbro commonly appears fractured with orthogonal fracture sets infilled by ultramafic rock made up of a blackish-brown olivine-rich matrix with rare apatite, magnetite and carbonate (Fig. 8G). The contact between the ultramafics and the gabbro clasts is made up of a highly altered reaction rim (Fig. 8G) composed of talc-actinolite alteration, most likely after clinopyroxene. Throughout the complex the olivine-rich rocks have been highly serpentinised and in localised zones strongly altered to talc-carbonate.

5.2.3. Variability along strike from Enterprise to Voyager and Intrepid

The marginal unit (surrounding the central gabbro) is not consistent in composition or thickness, and ultramafic rocks are commonly absent. Gabbro is the dominant rock of the marginal unit and, at Enterprise, is thickest and most abundant in the upper levels of the mine, whereas ultramafic rocks become relatively more abundant and increase in thickness with depth, in correlation with the amount of sulfide present. Sulfide at Munali demonstrates a clear spatial relationship with the ultramafic phases throughout the intrusive complex. Enterprise, situated in the south-eastern margin, contains the most economic concentrations of sulfide, being the site of the Munali mine. Two additional sulfide prospects, Voyager and Intrepid (Fig. 2) are also present along the south-western margin of the complex, however ultramafic rocks and sulfide are less abundant in comparison to Enterprise (Blanks et al., 2022). The ultramafic-sulfide relationship is persistent, whereby the abundance of ultramafic rocks correlates with the amount of sulfide and, at Voyager and Intrepid, minor intervals of sulfide breccia are associated with narrow ultramafic intrusions. Consequently, sulfide is not abundant consistently throughout the entire complex, although where present, displays similar sulfide and gangue mineralogical compositions and brecciation textures.

6. Nature of the Munali orebody

The Munali orebody at Enterprise (Fig. 4) appears to represent a typical sulfide-matrix breccia deposit, with brecciation constrained to the marginal units and along the contact with central gabbro. Sulfide is mainly composed of massive (>90 % sulfide) and semi-massive (90–20 % sulfide) ore comprising a sulfide assemblage of pyrrhotite and pentlandite with variable chalcopyrite and pyrite, alongside apatite and carbonate gangue. Mapping of the sulfide occurrences underground have revealed that on a macro-scale, the bulk of this sulfide is largely present as massive to semi-massive sulfide 'lenses' i.e. elongated, planar sulfide bodies orientated parallel to the intrusive complex strike. The thickest lens of the orebody is present at the base of the marginal unit; defined here as sulfide lens 1 (SL1) and is most commonly associated with (apatite)-magnetite-dunite at the contact with the unmineralised central gabbro. The SL1 is complemented by the addition of two to three similarly orientated, but thinner (<5 m) sulfide lenses (SL2 and SL3)

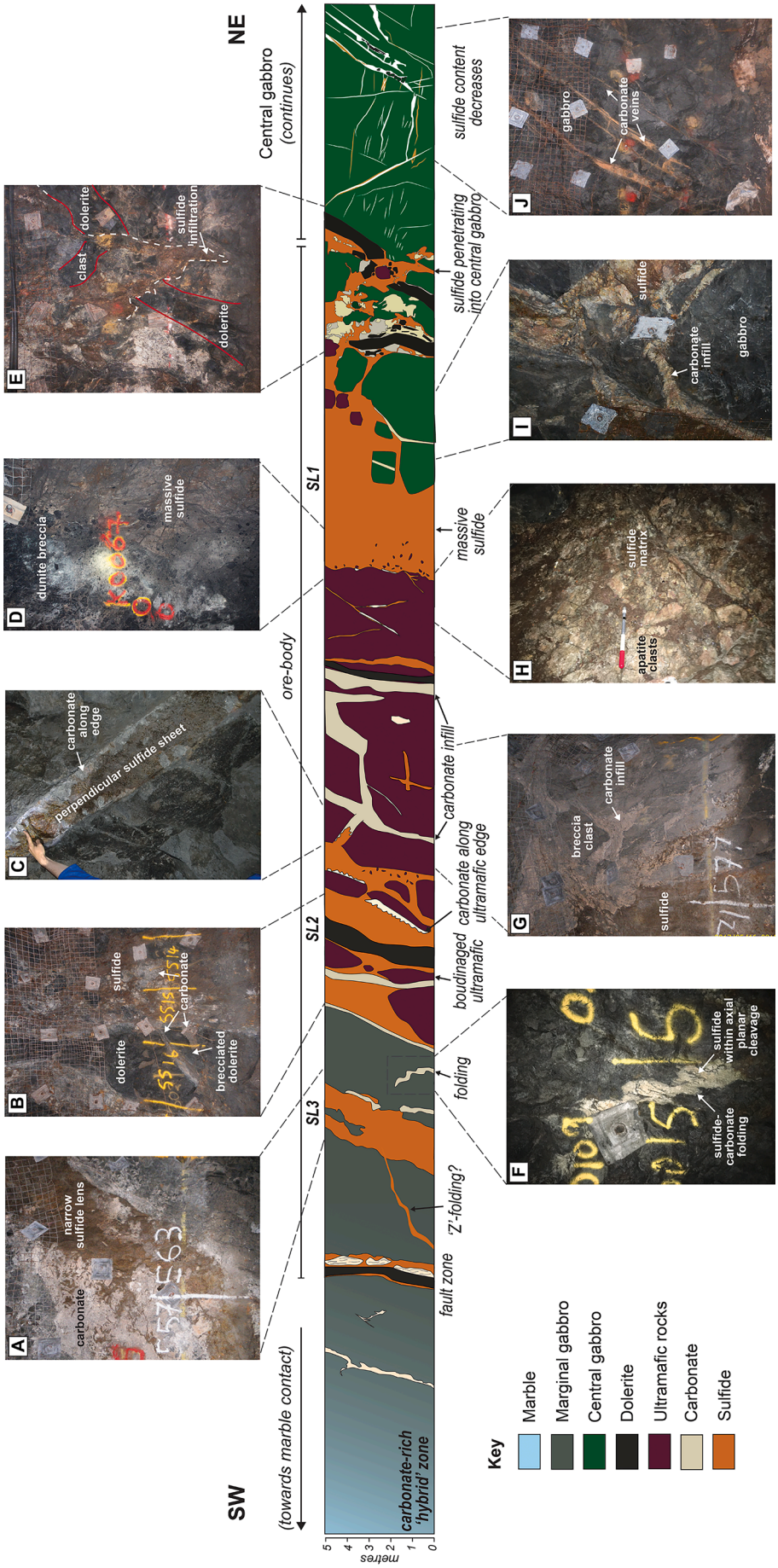

Fig. 4. Schematic cross-section of the Enterprise ore body mapped across the mine drives, showing location of sulfide and carbonate and relationship with host igneous rocks. Description of insets: A) sulfide lens (SL3) within marginal gabbro; B) dolerite boudin within carbonate-rich sulfide; C) perpendicular sulfide lens in dunite with pegmatic carbonate along dunite contact; D) rounded ultramafic clast hosted within massive sulfide of SL1; E) sulfide infiltration into central gabbro with hard-walled brecciation of dolerite and gabbro; F) parasitic folding of sulfide-bearing carbonate within gabbro; G) mafic–ultramafic breccia hosted by carbonate adjacent to sulfide; H) coarse apatite hosted within sulfide at contact of SL1 and ultramafic rocks; I) carbonate-sulfide infiltrating and brecciating central gabbro; J) orthogonal sulfide-poor carbonate veins in central gabbro.

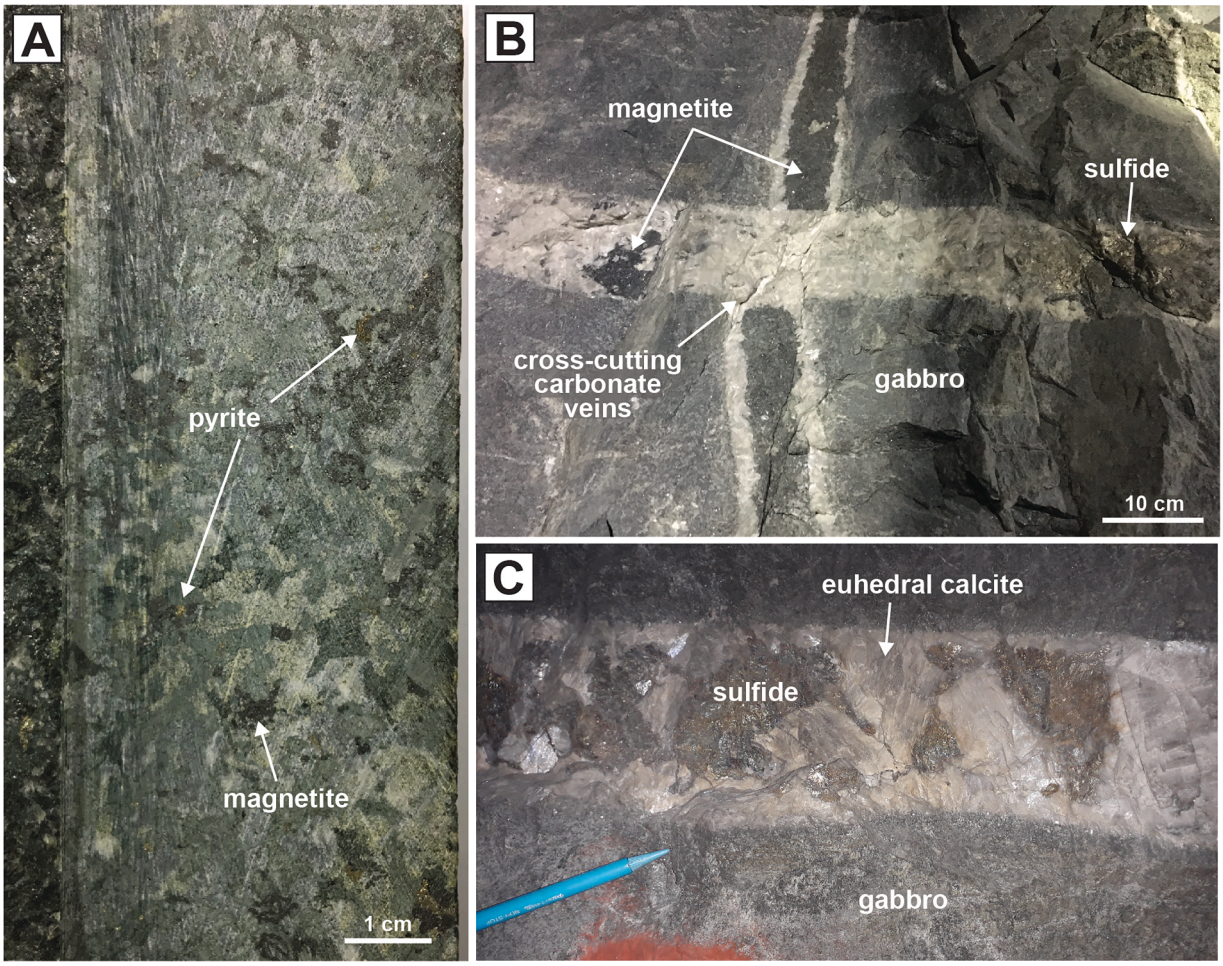

Fig. 5. Central gabbro and carbonate-sulfide footwall veins; A) altered poikilitic textured gabbro with fine disseminated pyrite; B) cross-cutting sulfide-magnetite-carbonate veins hosted within central gabbro; C) sulfide-bearing carbonate vein with coarse euhedral calcite crystals with interstitial sulfide (pyrrhotite-pentlandite-pyrite).

present towards the core of the marginal unit (Fig. 4).

6.1. Sulfide lenses of the Enterprise orebody

Sulfide lens 1 (SL1) represents the main sulfide body and is variable in thickness (1–30 m) both along strike and with depth, with the orebody appearing to exhibit a pinch and swell morphology. These sulfide lenses dip ~ 70-80° to the SW (Fig. 4), parallel with the intrusive contacts and bedding of the host metasedimentary sequence. Within SL1, sulfide-matrix brecciation is well developed, with fractures that propagate ~ 5 m into the central gabbro footwall (Fig. 4E,I). These fractures are infilled by a pyrrhotite-rich massive sulfide matrix. The clasts hosted by the sulfide in SL1 are principally comprised of dunite, central gabbro (towards the footwall contact) and lesser gabbro and dolerite of the marginal units. Additional gangue phases within the sulfide matrix ore breccia include a range of carbonates (calcite, dolomite and magnesite), apatite and magnetite (Blanks et al., 2022).

However, SL2 and SL3 differ from SL1, not only in their thickness, but also in the percentage and type of gangue clast phases, having a higher clast to sulfide ratio, with significantly higher percentage of carbonate. Accompanying the sulfide lenses are additional perpendicular sulfide veins (Fig. 4C,E,I), dipping approximately 20-50° to the north-east that are consistently narrower < 0.5 m thick, sometimes associated with observed displacement within the host-lithologies (Fig. 4E).

6.2. Carbonate-sulfide veins

Sulfide bearing carbonate veins, previously described by Holwell et al. (2017), are interpreted to represent a late mineralisation phase and are notably abundant within the central gabbro footwall. These veins, primarily calcite and/or dolomite are host to magnetite alongside accessory sulfide (Fig. 5B,C). These carbonate vein-sets are narrow in width (<20 cm) and are most abundant within the first 15 m of the footwall central gabbro where they occur approximately every 2–3 m (Fig. 4). However, they become less frequent away from the marginal contact towards the centre of the central gabbro where they become more carbonate and less sulfide dominant (Fig. 4). These veins also occur within the marginal units, and are either similarly orientated or perpendicular to the main sulfide lenses, although contain substantially less sulfide.

6.3. Sulfide brecciation

Detailed geological and structural mapping in this study have highlighted not only structurally controlled planar sulfide lenses but distinct brecciation styles that can be divided into 'hard-walled' and locally developed 'soft-walled' classifications.

6.3.1. 'Hard-walled' brecciation

'Hard-walled' brecciation is defined by the presence of sharp silicate-sulfide contacts (at the scale of the grain size of the silicate rock)

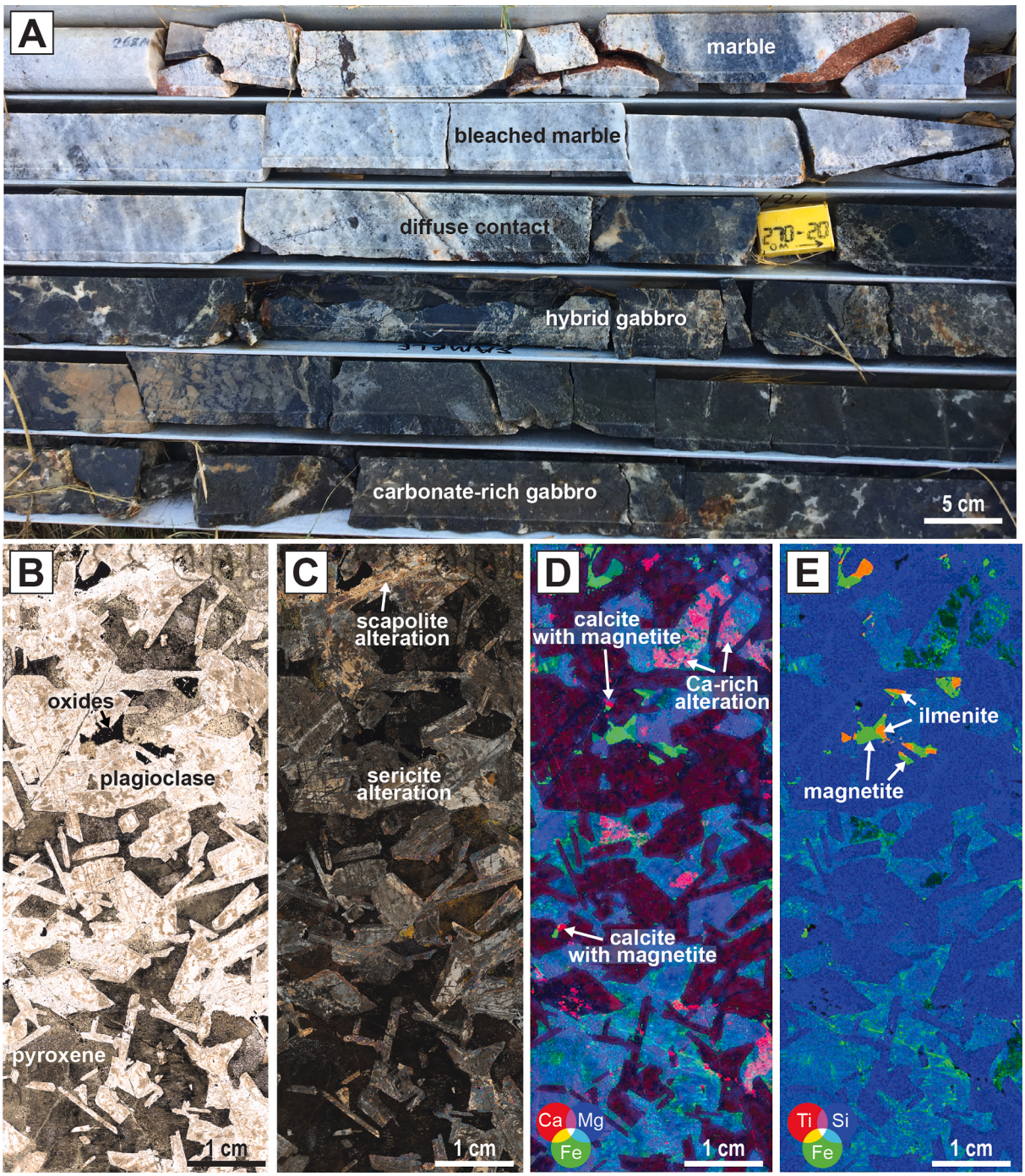

Fig. 6. Marginal gabbro; A) diffuse contact between marginal gabbro of the Munali Igneous Complex and host metasedimentary rocks, showing bleached white marble and carbonate-rich hybrid gabbro; B-E) marginal poikilitic gabbro; B) transmitted plane polarised light; B) transmitted cross polarised light; C) XRF Tornado^{TM} chemical map showing iron in green, magnesium in blue and calcium in red; highlighting extent of pyroxene alteration; D) XRF Tornado^{TM} chemical map showing iron in green, silica in blue and titanium in red highlighting interstitial magnetite and ilmenite and absence of sulfide. (For interpretation of the references to colour in this figure legend, the reader is referred to the web version of this article.)

indicative of fracturing of the silicate rock component in the absence of melting or disaggregation of clasts (Barnes et al., 2018). Hard-walled brecciation is the most pervasive of the breccia styles at Munali and occurs in conjunction with the massive sulfide lenses. This style of brecciation is characterised by large > 0.5 m angular blocks of gabbro, dolerite and rarely ultramafic rocks, from both the marginal and central units, hosted by a sulfide matrix (Fig. 9). Hard-walled brecciation is pervasive throughout the intrusive complex but is most commonly observed at the contact of the marginal and central units associated with SL1.

The angular clasts are commonly surrounded by a rim of crystalline carbonate and talc-carbonate forming along the brecciated edges that is then infilled with sulfide (Fig. 9A,B). The angular clasts display consistent orientations of fragmentation, forming rectangular blocks with two distinct orthogonal orientations to the fractures (Fig. 9), similar to that shown in Fig. 8G, that suggest brittle extension as a control to brecciation, with no clear evidence of significant spatial disaggregation. In Fig. 9, the fracture fill is sulfide, whereas in Fig. 8 it is ultramafic

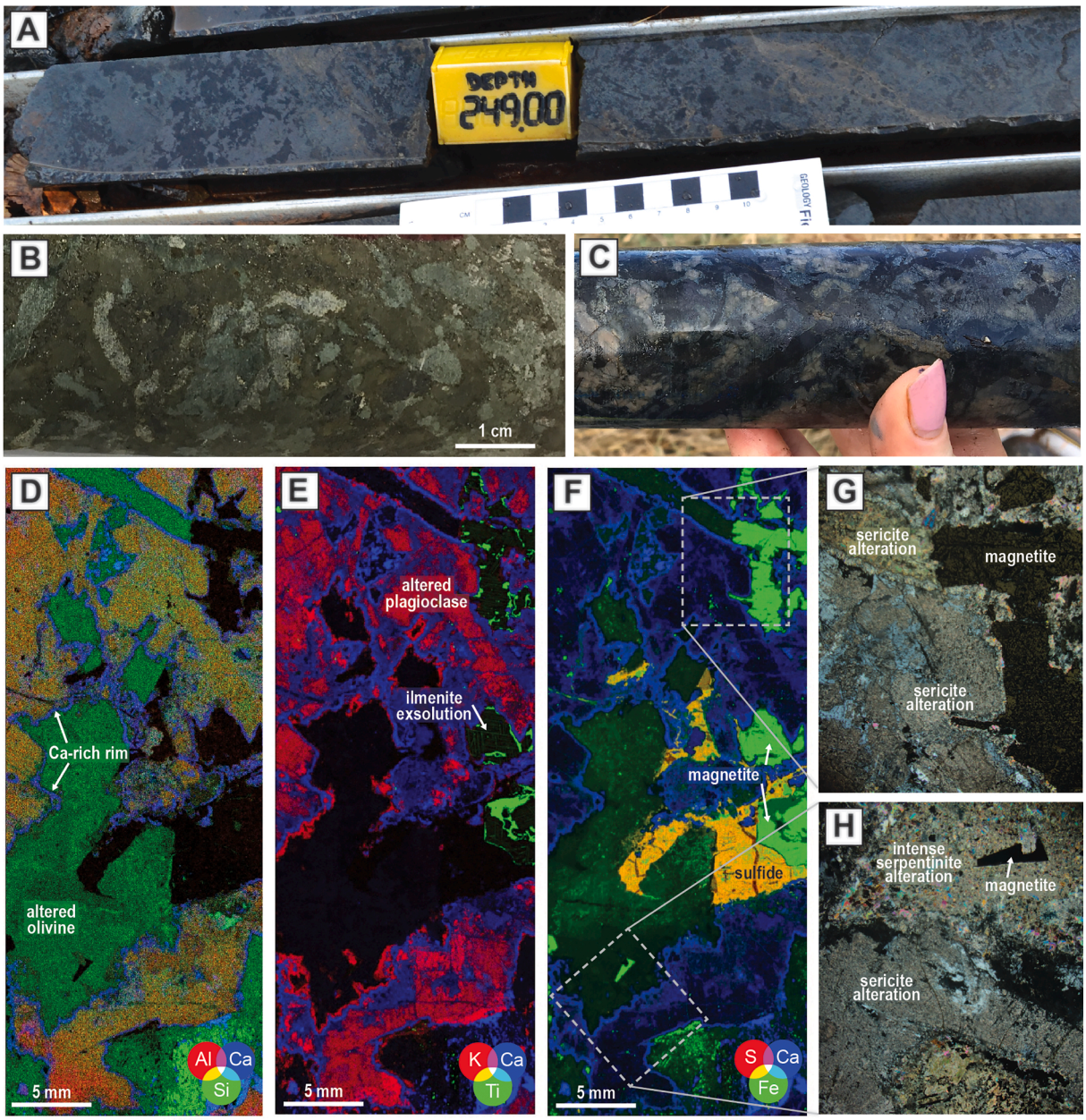

Fig. 7. Variably textured olivine gabbro in the marginal unit; A-C) patchy olivine-gabbro in drillcore in close proximity to dunite; D) XRF Tornado^{TM} image showing calcium in blue, silica in green and aluminium in red, highlighting presence of serpentinised olivine and calcium alteration rims; E) XRF Tornado^{TM} image showing calcium in blue, titanium in green and potassium in red, highlighting Ca-alteration of plagioclase; F) XRF Tornado^{TM} image showing calcium in blue, iron in green and sulfur in red, highlighting presence of sulfide (orange) and magnetite (light green); G-H) transmitted cross-polarised light showing extreme alteration of olivine-gabbro. (For interpretation of the references to colour in this figure legend, the reader is referred to the web version of this article.)

material, though both cases clearly show early fractures in gabbro being utilised by late ultramafic and sulfide melts.

6.3.2. *'Soft-walled' brecciation*

This style of brecciation, occurring on a smaller, mm-cm scale, is distinguished by the curvilinear contacts between sulfide and clasts (Fig. 10) and disaggregation of silicate clasts along original grain boundaries into the sulfide matrix (Barnes et al., 2018). Soft-walled brecciation is mainly confined to the ultramafic rocks (>80 % of clast fragments), whereby rounded to sub-angular ultramafic clasts derived from disaggregation of the adjacent apatite-bearing ultramafic rocks. The clasts have smooth edges and generally no preferred alignment comprising serpentinised olivine fragments and apatite with sub-rounded to circular morphologies (Fig. 11), and are hosted by the pyrrhotite-rich sulfide ore matrix.

Additionally, sulfide droplets are noted to wet along the edge of the apatite crystals (Fig. 11B,C). Notably, the clasts are present in higher concentration in sulfide towards the margins of the sulfide lens-ultramafic rock contact, from which the clasts have likely been dis-aggregated, suggestive of in-situ brecciation as opposed to, for example, an origin from a gravity flow of an inclusion-rich sulfide slurry.

6.4. *Orebody deformation*

In addition to the intense deformation of the metasedimentary rocks, deformation is also observed within the intrusive complex and best exposed underground at Enterprise. Frequent vertical dipping (~90°) NW-SE trending fault planes are present as narrow zones typically

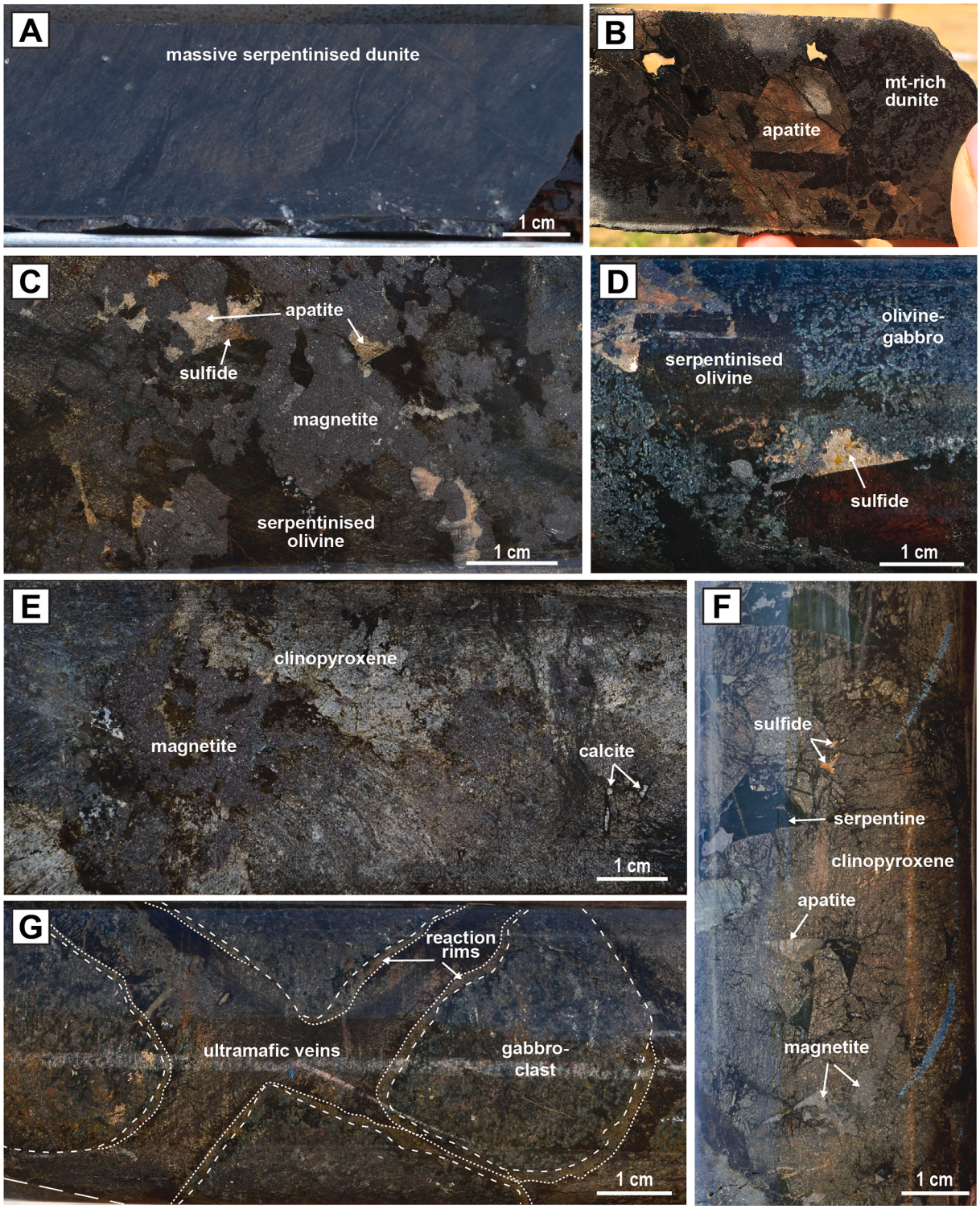

Fig. 8. Ultramafic rocks of the Munali Intrusive Complex. A) massive altered dunite; B) magnetite-rich dunite with coarse apatite and interstitial calcite; C) apatite-rich dunite with interstitial and late-style magnetite; D) interstitial sulfide vein in dunite within olivine-gabbro; E) magnetite-bearing wehrlite with interstitial calcite; F) apatite-bearing clinopyroxenite with minor interstitial sulfide; G) ultramafic veins within a fractured-brecciated gabbro with reaction rims.

20–50 cm wide (Fig. 12A) that cross-cut earlier sulfide brecciation. These fault planes are infilled with talc-carbonate, where magnesite is the dominant carbonate phase, and in places completely altered to soapstone, with some associated chalcopyrite-pyrrhotite-rich sulfide. The fault zones are dominated by linear fabrics of carbonate and sulfide, orientated parallel to the fault plane. Deformation of the orebody is best observed in sulfide sheets SL2 and SL3, where sulfide is regularly dominated by carbonate-rich sulfide breccia (Fig. 4A,B,F,G and Fig. 12). Occasional parasitic folding and boudinage of the marginal rocks present as sub-vertical arrays (Fig. 4B,F and 12B-D), with gabbro and apatite forming the rigid boudin centres (>5 cm) surrounded by carbonate-sulfide (Fig. 12B and C).

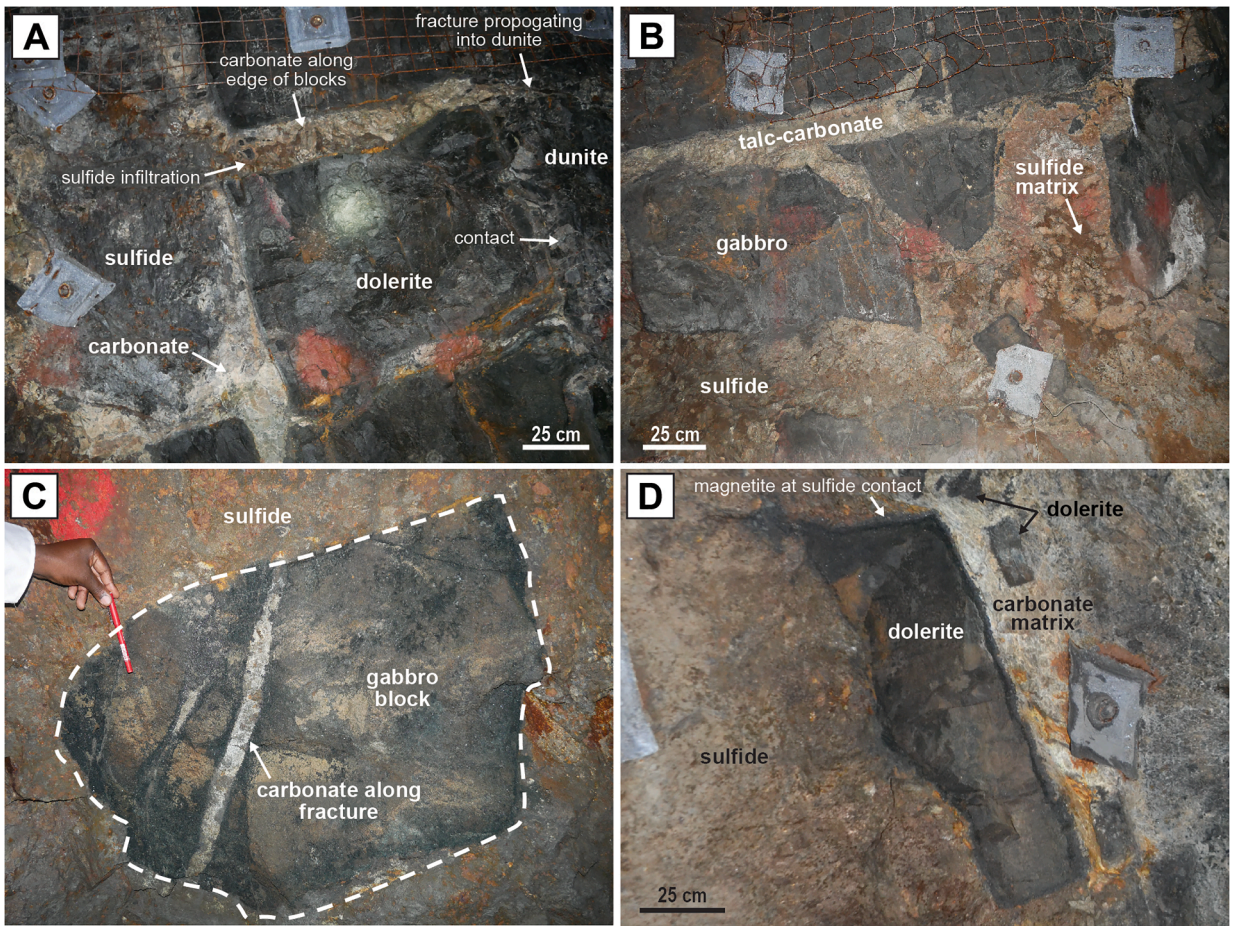

Fig. 9. Hard-walled macro brecciation textures. A) Brecciated dolerite in contact with lesser brecciated dunite. Carbonate is present along the edges of the brecciated blocks with massive sulfide matrix; B) brecciated central gabbro hosted by sulfide and carbonate, with carbonate preferentially along the edges of the breccia blocks; C) breccia block showing multiple stages of deformation, with initial carbonate infilling the gabbro fragments hosted within the massive sulfide matrix; D) blocky dolerite adjacent to carbonate hosted by massive sulfide.

7. Whole-rock geochemistry

The bulk rock geochemistry of the different intrusive phases within the Munali complex is shown in Fig. 13. Major element analysis of the intrusive rocks show that the different rock types each have their own distinct geochemical signatures and exhibit variable MgO contents (Fig. 13), reflecting the abundance of olivine and pyroxene, as a component of the modal assemblage. The ultramafic suite, which includes wehrlite and dunite, display the highest MgO and lowest SiO_2, due to the modal mineralogy dominated by olivine, and plot as a cluster, whereas the mafic suite form linear trends with decreasing MgO contents from olivine-gabbro, dolerite, marginal gabbro to the central gabbro (Fig. 13A).

The FeO is variable, but slightly increases with increasing MgO contents towards the ultramafic rocks, reflecting the higher olivine, sulfide and magnetite abundance compared with mafic rocks (Fig. 13B). The Al_2O_3, K_2O + Na_2O and TiO_2 content generally decrease with increasing MgO content and similarly display linear trends reflecting a decrease in plagioclase and ilmenite abundance (Fig. 13C-E). The CaO content is generally consistent for the mafic rocks, between 6 and 12 wt %, with the exception of the olivine-gabbro which has lower and more variable CaO contents, between 2 and 8 wt% (Fig. 13F), whereas the ultramafic rocks generally display < 2 wt% CaO, with the exception of wehrlite, which reflects the presence of significant clinopyroxene. Nickel in sulfide-poor rocks shows a general increase with MgO content, with a positive correlation from central gabbro to wehrlite (Fig. 13G). Dunites show a spread in Ni content (333–784 ppm) for relatively consistent MgO (25.9–32.8 wt%). Chromium in the mafic rocks shows a positive trend with increasing MgO, from the central gabbro (Cr < 138 ppm) to olivine gabbro (Cr 161–502 ppm), but unlike other geochemical trends (i.e. MgO vs TiO_2; Al_3O_3; N_2O + K_2O), this is not continued into the ultramafic rocks; that instead plot as a separate cluster with exceedingly low Cr (<125 ppm).

The chondrite-normalised rare earth element (REE) profiles of the mafic rocks generally show similar flat-lying trace element patterns (Fig. 14A), with La/Yb ratios of 1.05–1.35 with the exception of the olivine-gabbro which displays higher La/Yb ratios of 1.46–4.8. Rare earth element concentrations are an order of magnitude higher than chondrite values and are very slightly enriched in light REE (LREE) relative to (mid-ocean ridge basalt) MORB (Fig. 14B). Notable depletions in Eu, with the exception of the olivine-gabbros, likely highlight previous crystallisation and removal of plagioclase. The REE patterns of the ultramafic rocks are more variable between the different rock types (Fig. 14C). Wehrlite shows a similar flattened profile to the mafic rocks suggesting a similar source, but show enrichments in Yb and Lu.

The dunites display-two contrasting profiles depending on P_2O_5 content (Fig. 14C); apatite-poor dunites show a U-shaped concave profile (below chondritic values), with a depletion in the middle REE (MREE) relative to the LREE and heavy REE (HREE) (La/Sm of 1.9 to 20.3), which is effectively the composition of the olivines given the bulk mineralogy. The apatite-rich dunite, however, shows more enriched REE profiles for all elements, suggesting apatite significantly influences the REE content in the rocks. The ultramafic lithologies similarly show notable depletions in Eu, with the exception of dunite, which shows

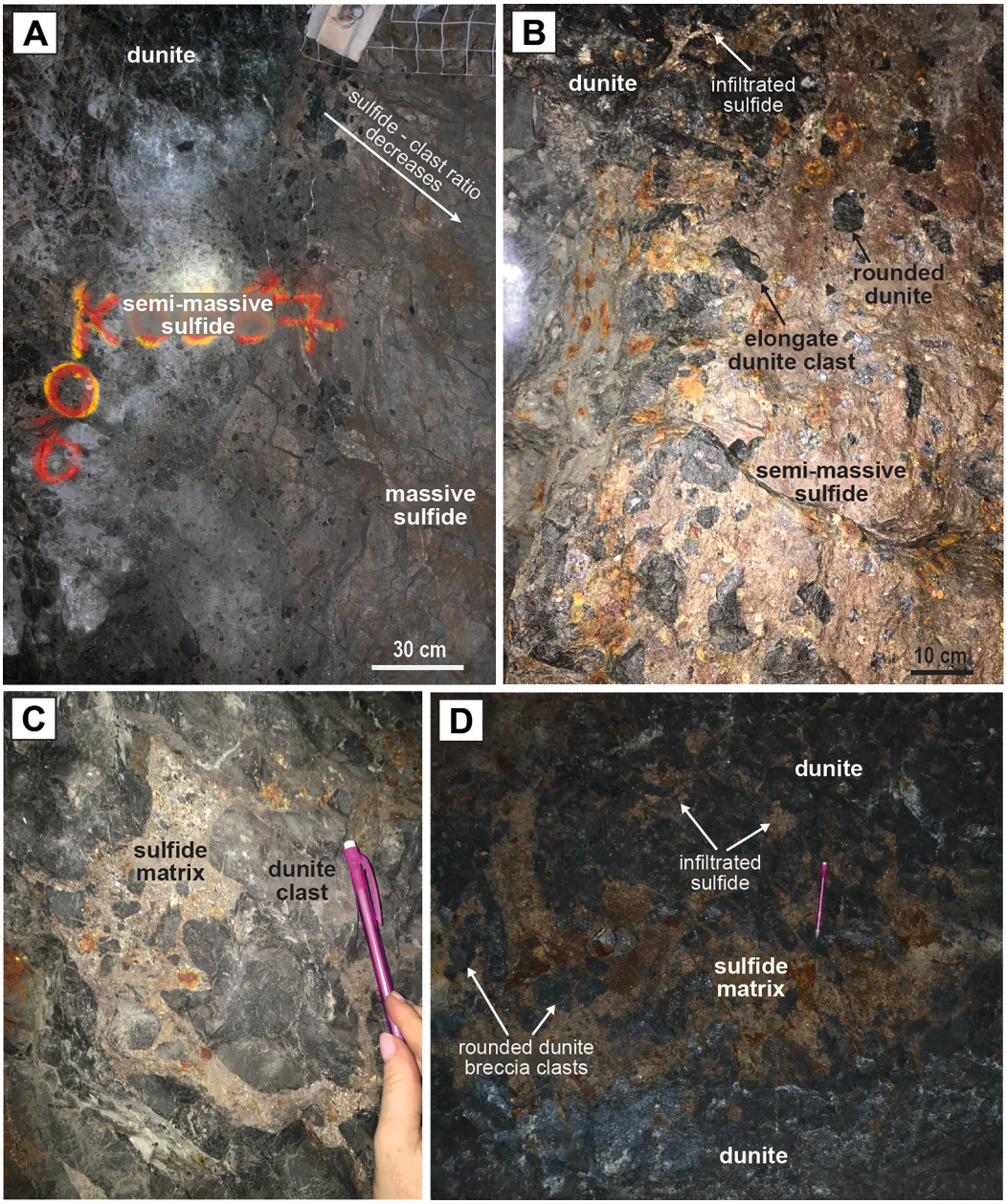

Fig. 10. Soft-walled brecciation textures. A) Gradation of sulfide breccia at contact of massive sulfide with dunite, becoming less clast dominated away from contact; B) rounded dunite clasts hosted by sulfide matrix; C) rounded dunite clasts of variable size hosted by sulfide at the sulfide-dunite contact; D) passive sulfide infiltration of sulfide along contact with dunite.

slight depletions, with two samples anomalously enriched. Multiple trace element plots normalised to MORB (Fig. 14B and D), show distinct enrichment of the low field strength elements, Rb, and Pb, which are elements that are easily mobilised in hydrothermal and/or serpentinised altered rocks.

8. Apatite chemistry

Apatite is characteristically coarse grained (>0.1 – 30 cm length) and is present in three associations: (1) as an interstitial phase of the ultramafic lithologies (Fig. 15A) (2) as rounded to subhedral crystals hosted by sulfide (Fig. 15B); and (3) as apatite veins in dolerite (Fig. 15C). Texturally the apatite vary, and are either cloudy, or have clear cores and cloudy rims, yet the compositions of the apatite, in terms of REE, do not vary between apatite of different textures or from core to rim, even when an obvious zonation is apparent, nor do they show different chondrite normalised REE profiles between styles (Fig. 15D-F).

All styles display similar abundances of REE, with the mean profiles of ultramafic and sulfide associated apatite, being almost identical with the exception of Eu (Fig. 15), yet all show large, negative anomalies in Eu with Eu/Eu* between 0.02 and 0.69. All profiles display a moderate enrichment in LREE relative to HREE with La/Lu_N ratios between 4.1 and 23.3. As such, the textural styles are geochemically indistinguishable.

However, apatite within the Munali Complex can be exceedingly Cl-rich, (0.87 to 5.53 wt% Cl), with occasional greener F-rich apatite with F up to 1.87 wt%. Chlorine enrichment is not consistent throughout or within the different apatite styles (Fig. 16), which are either homogenously enriched, show Cl-rich rims (Fig. 16A-B) and/or Cl-rich cores (Fig. 16C) or are associated with fractures (Fig. 16F), regardless of host rock association (i.e. sulfide or ultramafic-hosted).

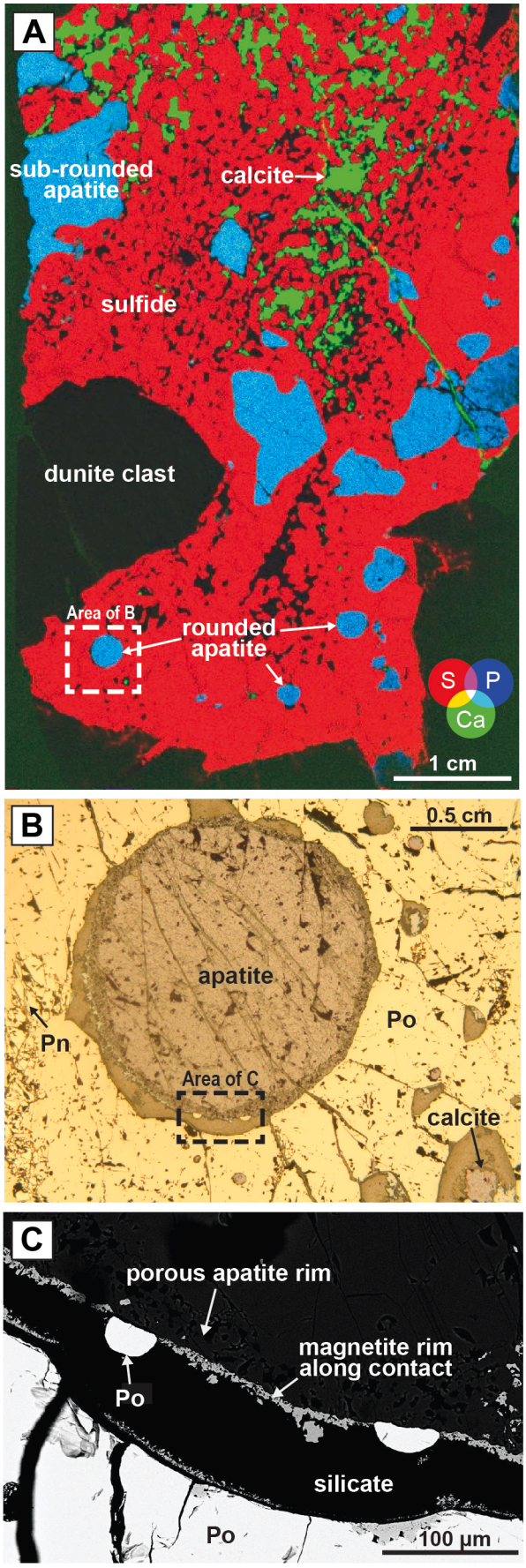

(caption on next column)

Fig. 11. Sulfide breccia host to sub-rounded ultramafic and apatite clasts; A) XRF Tornado™ image of semi-massive sulfide with ultramafic breccia clasts hosted within sulfide matrix, highlighting aggregated nature of serpentinised dunite clasts, and sub-rounded to well-rounded apatite and interstitial calcite; B) reflected and transmitted plane polarised reflected light image of rounded apatite with porous rim hosted in pyrrhotite (Po) and pentlandite (Pn) with sulfide droplets along apatite edge; C) SEM backscattered electron image of sulfide droplets shown in B wetting edge of apatite at contact with silicate hosted in sulfide matrix with magnetite rim along contact of apatite.

9. Carbonate C-O isotopic characteristics

Carbonate is a characteristically ubiquitous phase of the sulfide mineralisation at Munali and is present in a range of compositions and textures, as (Fe)-dolomite, ankerite (Fe-Mn-dolomite), calcite, and magnesite (Fig. 17). Calcite is spatially associated with the ultramafic rocks, with rare calcite within the apatite-rich dunites, where it is present as inclusions within apatite, or interstitially to the apatite and olivine (Fig. 17A). Calcite also occurs as an interstitial phase to semi-massive sulfide, where sulfide exhibits blebby textures within a carbonate interstitial network, rimmed by an extremely fine-grained silicate at the sulfide-calcite contact (Fig. 17B,C). Dolomite, however, is the most directly associated with the ore sulfide, commonly occurring in SL2 and SL3, and texturally occurs as massive patches or as rare euhedral calcite/dolomite crystals hosted by sulfide (Fig. 17D,E). Additionally, rare dolomite, in euhedral or interstitial form, has been observed to host to sulfide blebs containing pentlandite-chalcopyrite loop textures (Fig. 17) that are evidence for primary magmatic rather than a tectonic origin (Barnes et al., 2020b).

In the central gabbro, calcite is also present alongside dolomite as thin veins of carbonate-sulfide-magnetite (Fig. 4J and 5B) in propagating fracture sets present up to 50 m away from the orebody. Talc-carbonate altered rocks throughout the marginal zone contain magnesite as the dominant carbonate, commonly occurring alongside talc, associated with fault planes and in highly serpentinised zones (Figs. 4 and 17G), most concentrated towards the hanging wall contact where there is the clearest evidence of post-sulfide emplacement deformation.

Seventy C and O isotope analyses were undertaken on calcite, dolomite and magnesite from the ultramafic-rocks, sulfide ore assemblage and carbonate-bearing country rocks (Table 1). The number of samples analysed from within the Munali Complex were taken on the abundance and availability of different carbonate styles (Fig. 17). Following the previous suggestion for a carbonatite affinity at Munali and classification of ultramafic rocks as phoscorites (Holwell et al., 2017), eleven samples from the nearest carbonatite, Keshya (Fig. 1), and phoscorites of the carbonatite intrusive complexes at Kovdor, Russia and Phalaborwa, South Africa were analysed for comparison.

The calcite within the ultramafic rocks, present as an interstitial phase and as inclusions within apatite, define a population with the lightest $\delta^{13}C$ of ~ -4 ‰ and $\delta^{18}O$ of ~ +4.5 ‰ (Table 1). Three separate carbonate associations have been characterised with sulfide ore and display variable signatures (Fig. 18). Interstitial calcite, show $\delta^{13}C$ of −6 to −7.5 ‰ and $\delta^{18}O$ of + 6 to + 10.5 ‰ (Fig. 18; Table 1). The bulk of the carbonate with sulfide (predominately as dolomite and magnesite) forms a broad but well defined range with $\delta^{13}C$ between 0 ‰ and −4 ‰ and $\delta^{18}O$ between + 8 ‰ and + 14 ‰ (Fig. 18). Magnesite, part of the talc-carbonate assemblage associated with sulfide, shows similar $\delta^{13}C$ values to the dolomite-sulfide between 0 to −4 ‰ but variable $\delta^{18}O$ of + 9 to + 15.5 ‰ (Fig. 18).

The carbonate of the country rock marbles shows a spread in both the $\delta^{13}C$ and $\delta^{18}O$ values between −0.5 to + 5 ‰ and + 15 to + 28 ‰ respectively (Fig. 18; Table 1), and evidently represents the most isotopically heavy carbonate phase. Calcite from the Keshya carbonatite (60 km to the E of Munali) display negative $\delta^{13}C$ of −3 and −4‰ and distinctively lighter $\delta^{18}O$ of + 1 to + 5 ‰ (Table 1) than that of mantle carbonate and known carbonatites (Deines, 1989; Jones et al., 2013).

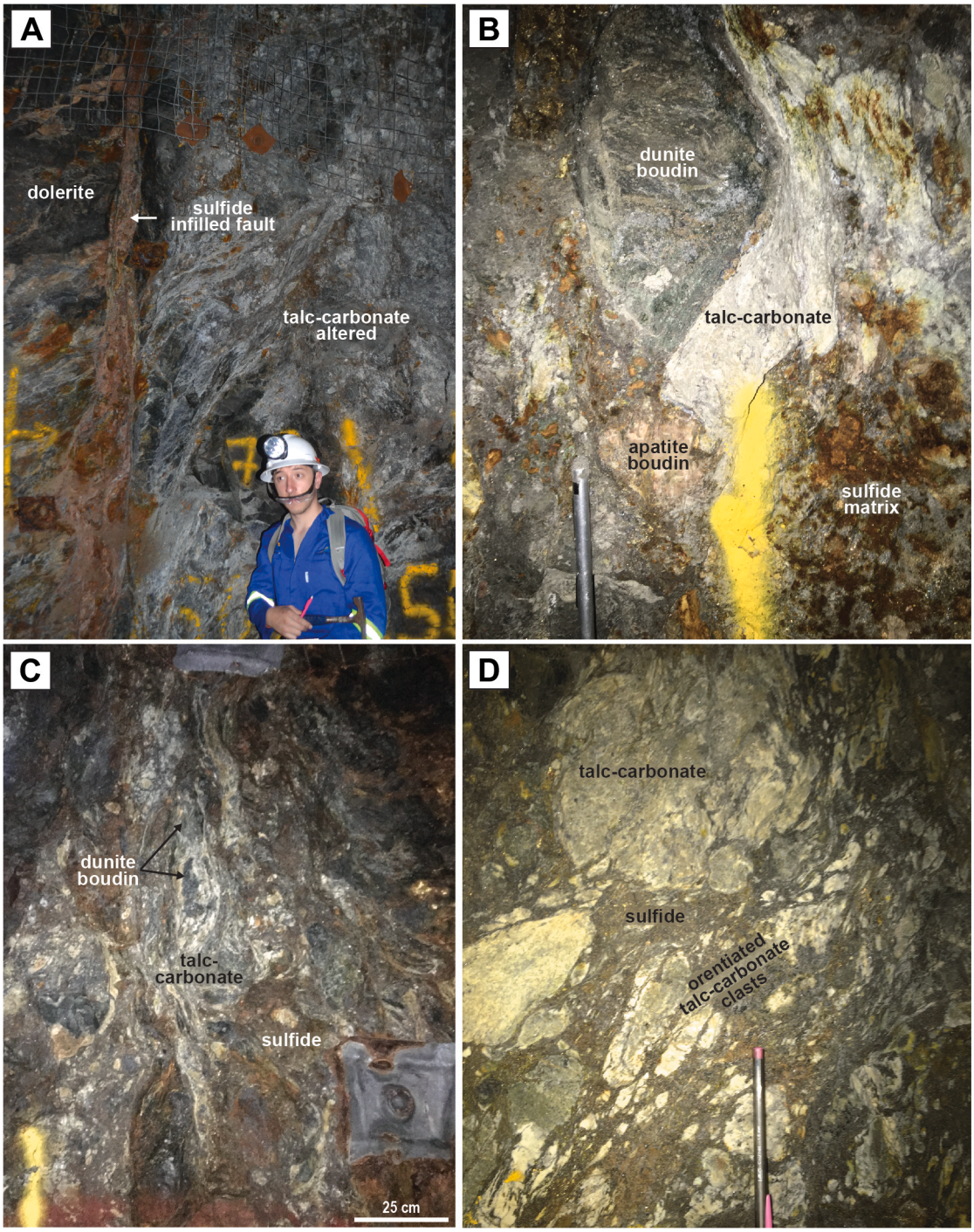

Fig. 12. Deformation of the orebody at the Enterprise mine. A) Fault zone within carbonate-rich mafic rocks with vertical fault infilled with sulfide; B) boudinaged dunite and apatite hosted by carbonate-rich sulfide matrix, with carbonate showing strong foliation aligned with boudined clasts; C) boudinaged dolerite and dunite hosted by talc-carbonate and carbonate-rich sulfide; D) carbonate-rich sulfide with carbonate showing strong curvilinear foliation.

Calcite analysed within phoscorite from carbonatite complexes Kovdor and Phalaborwa show similar $\delta^{13}C$ between −1.7 to 3.6 ‰ (Table 1), with slight differences in $\delta^{18}O$, with Kovdor between $\delta^{18}O$ + 6.3 and + 7.0 ‰, and Phalaborwa between $\delta^{18}O$ + 7.9 and + 14.6 ‰ (Table 1).

10. Discussion

The Munali Intrusive Complex (MIC) appears to represent a magmatic sulfide system that does not entirely conform to the current classifications of magmatic sulfide deposits, with atypical host rocks, gangue mineralogy and timing relationships. Detailed mapping and geochemistry builds upon previous work and now allows us to explain some of the outstanding questions pertaining to the nature and genesis of the deposit. We are able to place a number of constraints on the origin and relative timings of the abundant carbonate and apatite associated with sulfide, and subsequently the source of the magmas, alongside further timing constraints on the physical mechanisms that control brecciation, sulfide emplacement and deformation. We are therefore able to put forward a robust geological framework for the emplacement of both the igneous rocks, and the sulfide deposit they now host.

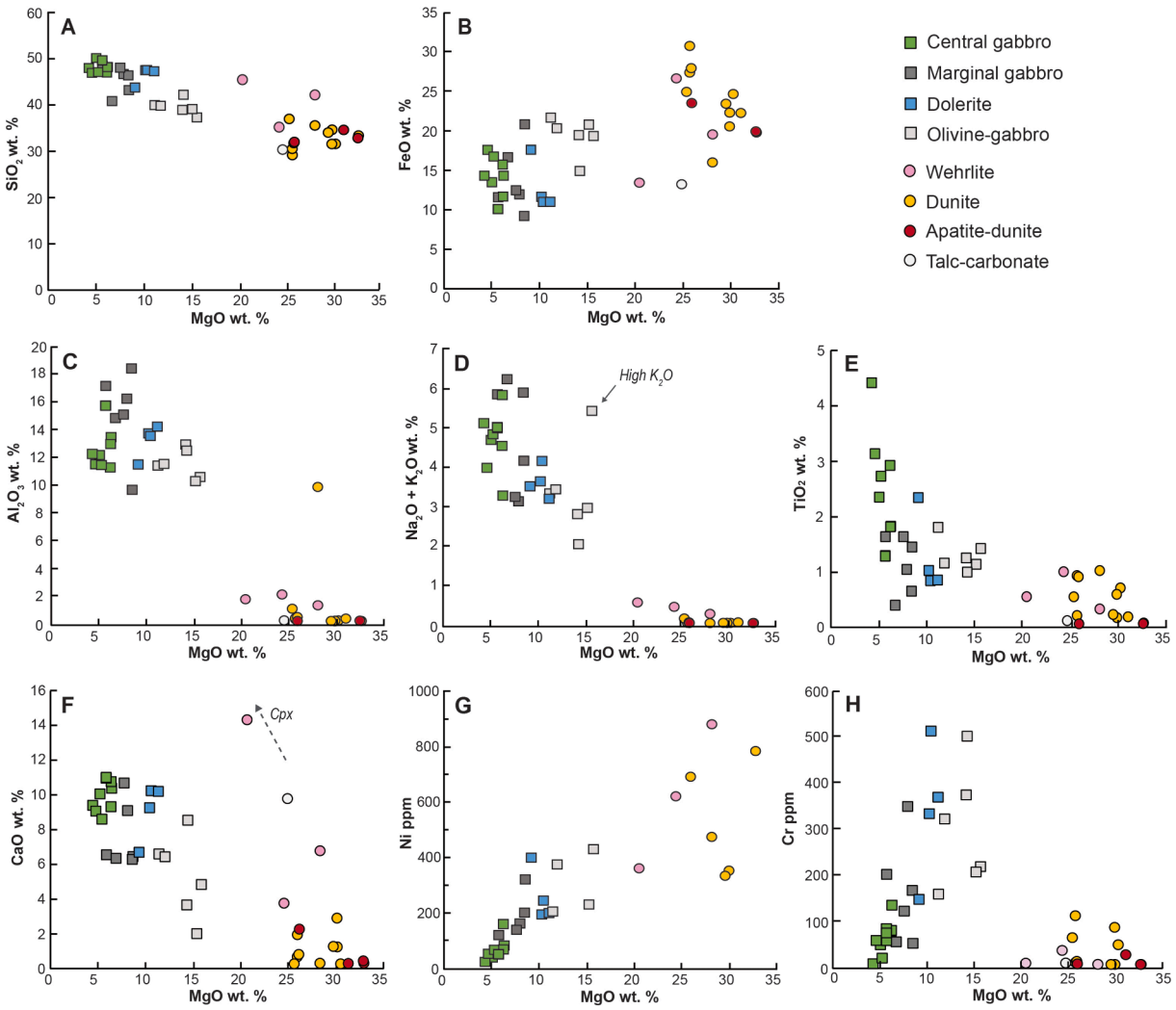

Fig. 13. Whole-rock geochemistry. A-E) Major element geochemistry binary variation diagrams for the igneous intrusions of the Munali Intrusive Complex of MgO vs A) SiO_2 B) FeO C) Al_2O_3 D) $Na_2O + K_2O$ E) TiO_2 F) CaO; G) Ni; H) Cr.

Although Munali may not conform to conventional host rocks to magmatic sulfide deposits in some respects, there is an increasingly broad range of recognised host rocks for magmatic sulfides, related to a number of tectonic settings. Advances in understanding the controls and emplacement of magmatic sulfide genesis has led to discovery and exploration potential in previously considered 'unprospective' intrusions and settings, such as mafic–ultramafic bodies in collisional orogenic belts, e.g. Aguablanca, Spain (Piña et al., 2010), Beja gabbroic intrusions, Portugal (Jesus et al., 2020), Ntaka Hill, Tanzania (Barnes et al., 2019) and deposits of the Central Asian Orogenic Belt in central China (e.g. Huangshandong; Deng et al., 2014). Additionally, there are some unconventional styles of magmatic sulfide mineralisation hosted by more alkaline and hydrous igneous complexes. These range from purely magmatic, such as lamprophyric intrusions (e.g. Sron Grabh, Scotland; Graham et al., 2017 and Mordor Complex, Australia; Barnes et al., 2008; Holwell and Blanks, 2021); to Cu-bearing alkaline-phoscorite-carbonatite complexes (e.g. Kovdor and Phalaborwa; Rudashevsky et al., 2004), and therefore a carbonatitic-phoscoritic origin for Munali is potentially plausible. Our combination of bulk rock geochemistry, apatite mineral chemistry and C-O isotopes allows us to test this hypothesis thoroughly.

10.1. The origin of carbonate at Munali

Based on their mineralogy, Holwell et al. (2017) suggested the apatite-magnetite rich dunites may be phoscorites; rare olivine-magnetite-apatite rocks that are nearly always associated with carbonatite-complexes (Krasnova et al., 2004). Phoscorites typically represent early differentiation of carbonate–silicate melts whereby early cumulates from the silicate portion of the magma comprise forsterite/diopside, magnetite and apatite. By extension, Holwell et al. (2017) also suggested that the abundance of carbonate and apatite at Munali, may be the result of the interaction of primary magmatic carbonatitic melts. However, it should be noted that as the MIC is emplaced almost entirely into a unit of marble, a crustal contamination source for the carbonate would seem likely. Here we use C-O isotopes of the carbonates within, and surrounding, the MIC to investigate a phoscorite and carbonatite source for the ultramafic rocks and the extent of crustal input into the abundant carbonate associated with sulfide.

Any interpretation of C-O isotope data requires full appreciation of any potential signature of local contaminants; which is of particular importance at Munali given the host rocks are carbonate metasedimentary rocks. However C-O isotope signatures of early Neoproterozoic carbonates within the Zambezi Belt are not well constrained. The local carbonates are thought to have been deposited during Zambezi rifting (~870 to 820 Ma; Hanson et al., 1994; Goscombe et al., 2020). Globally,

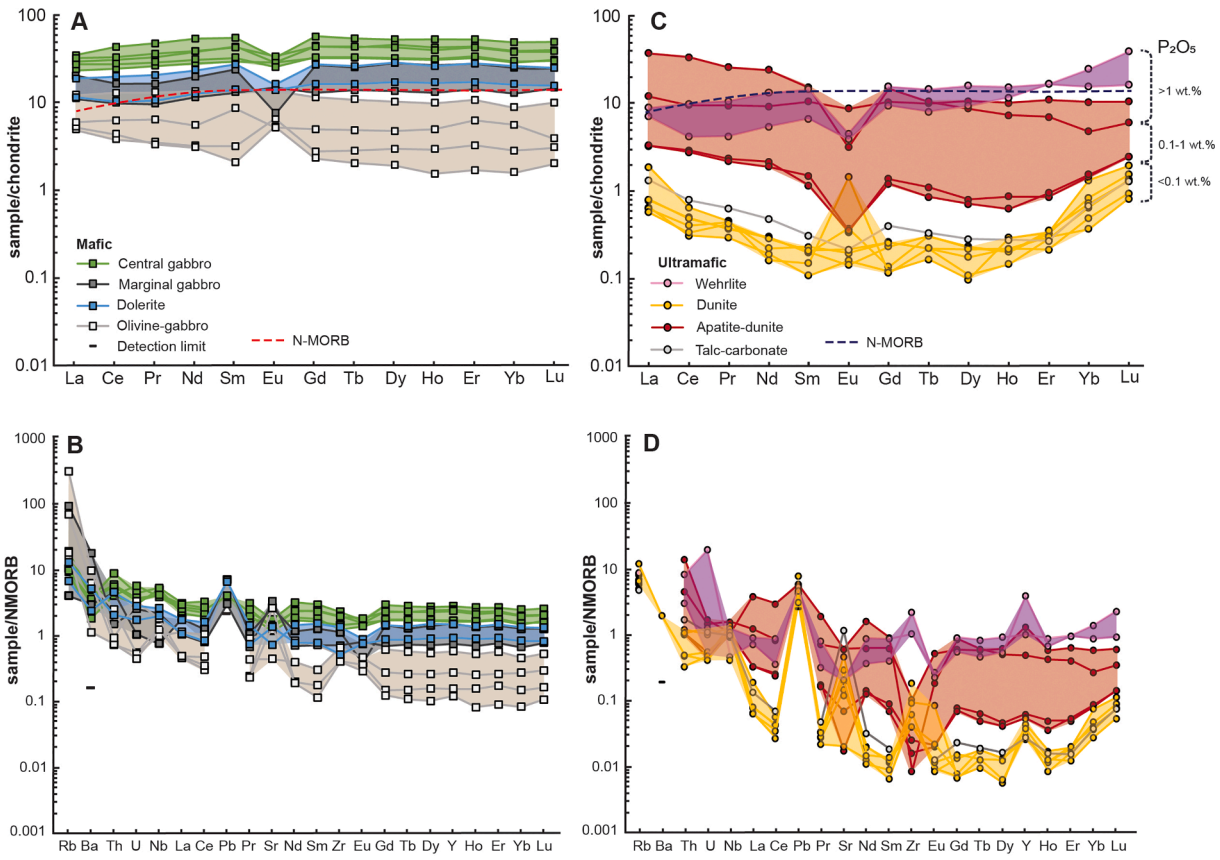

Fig. 14. Chondrite normalised (Sun and McDonough, 1989) REE element pattern and MORB normalised (Sun and McDonough, 1989) trace elements of the intrusions within the Munali Intrusive Complex (ranges shown in colour fields). A-B) mafic intrusions; and C-D) ultramafic intrusions, showing relative P_2O_5 content.

Neoproterozoic marine sediments typically show high average $\delta^{13}C$ values, with sharp negative anomalies (~-5 ‰ $\delta^{13}C$) associated with glaciation (e.g. deposition of the Sturtian Grand and Petit Conglomérat in the Copperbelt, Northern Zambia; Key et al., 2001). Importantly here, carbonate within the Roan and Nguba groups of the Katangan sediments of the Copperbelt (thought to be equivalent to the carbonate-rich host rock formations of the Cheta and Nega Formations in the Zambezi Belt; Johnson et al., 2007), displays distinct heavy sedimentary signatures with $\delta^{13}C$ and $\delta^{18}O$ values around + 5 ‰ and + 25 ‰ respectively (Bull et al., 2011). The local crustal signatures during the time of emplacement should therefore be isotopically heavy, and distinct from mantle values. The results of C and O isotope analysis from this study report the first isotopic signatures for Neoproterozoic sediments of the Zambezi Belt, which are isotopically heavy with fields of $\delta^{13}C$ of ~ 5 ‰ and $\delta^{18}O$ of ~ 25 ‰ (Fig. 19), identical to the Katangan sediments.

Carbon-oxygen isotope analysis of marbles were taken at varying intervals along strike and away from the MIC. These distal carbonate signatures fall within the distinct Neoproterozoic sedimentary field. However both the C and O isotope signatures of the metasedimentary rocks decrease towards the contact with the MIC (Fig. 19) highlighting the potential of high-temperature devolatilisation of C and O from the igneous complex, which would reduce the C-O isotope ratios. Nevertheless, they remain distinct from carbonate within the intrusive complex itself where multiple forms of carbonate are present (Fig. 17).

The majority of carbonate within the MIC is associated with sulfide as either crystalline dolomite, calcite, or as magnesite within talc-carbonate alteration assemblages. Calcite hosted interstitially to sulfide (Fig. 11A and 17B,C), shows the clearest mantle signatures (Fig. 19) as defined by Taylor et al. (1967), and highlights the clear presence of a primary magmatic carbonate component at Munali. Additionally, calcite present as a rare accessory component within the apatite-magnetite dunite (Fig. 8B,E and 17A), displays isotopic signatures of δC^{13} around −4‰ and δO^{18} between −4 and −5‰, just outside the defined mantle fields (Fig. 19). The signatures of the ultramafic-hosted calcite fall along a similar trend to that of the nearest carbonatite, Keshya (located 35 km to the east of Munali) that plots away to the left from the mantle field, with light δO^{18} signatures (Fig. 19); a trend suggested to be due to interaction with seawater or high-temperature meteoric fluids (Deines, 1989; Demény et al., 1998). In comparison to classified phoscorites, the C-O signatures analysed of calcite from the Kovdor and Phalaborwa phoscorite-carbonatite intrusions show δC^{13} signatures of around −3 to −4‰ (Zaitsev and Bell, 1995; Horstmann and Verwoerd, 1997), which plot above the defined mantle field and close to calcite signatures from the Munali ultramafic rocks, indicating a possible similar origin for the carbonate of the Munali dunites and other phoscorites globally.

Both dolomite (Fig. 17E) and talc-carbonate (Fig. 17G) associated with sulfide, falls isotopically between the mantle and sedimentary fields (Fig. 19). This would be suggestive of either: high temperature decarbonation of assimilated sedimentary rocks; mixing of a mantle (e.g. preserved in the dunite) and a sedimentary source, with the incorporation of heavier δC^{13} due to carbonate assimilation from the immediate country rocks; fractionation; or metasomatism of calcite (Fig. 19). This is entirely consistent with the S isotope study presented in Blanks et al. (2022), which shows a crustal S isotope signature in the Munali ores that is most likely to have been derived from S present within the same carbonate units that the complex is emplaced into. As such, these carbonates are an important source of both C and S to the overall Munali ore assemblages.

The C-O isotope signatures of calcite and dolomite associated with magmatic sulfides in alkaline intrusions in the lower and mid crust display mantle and carbonatite δC^{13} signatures with a trend towards that of local crustal signatures (Blanks et al., 2020). However, these rocks are

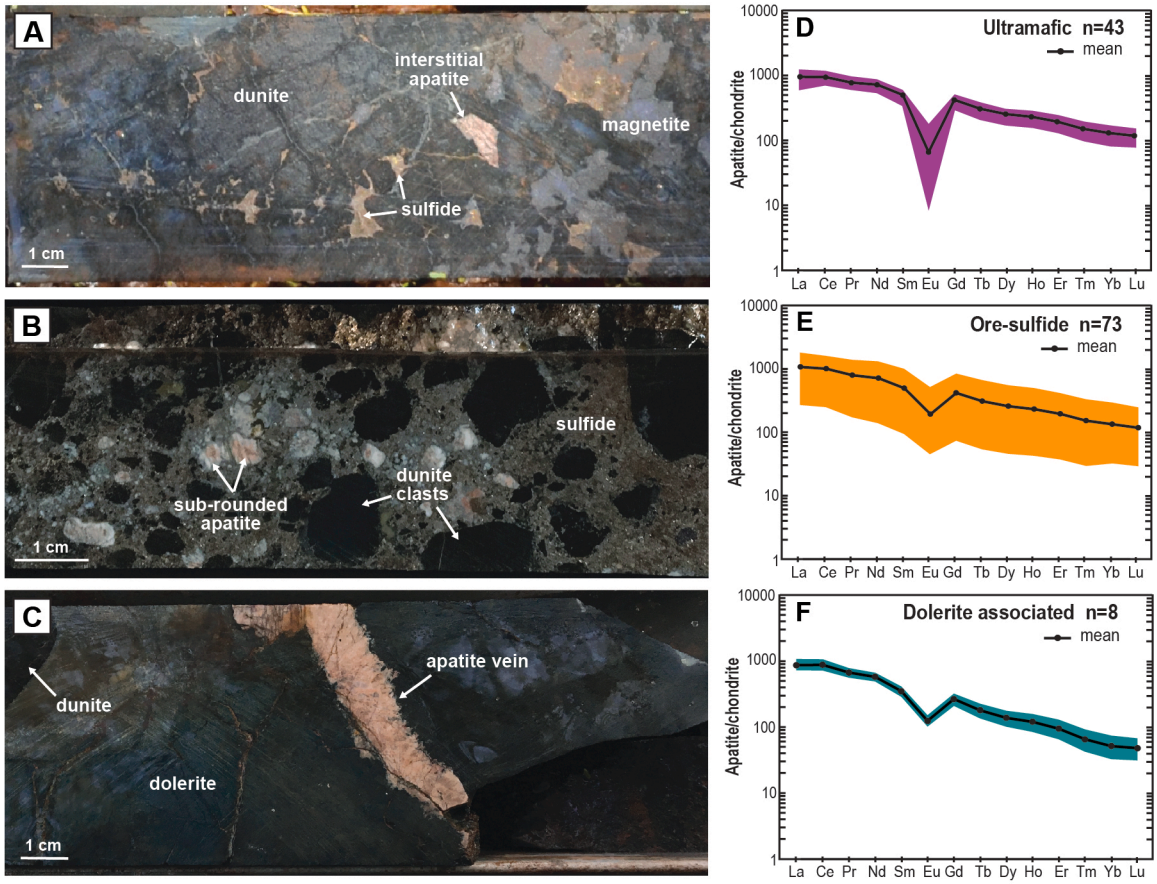

Fig. 15. Apatite styles of the Munali Intrusive Complex (A-C); A) apatite hosted interstitially within sulfide-bearing magnetite dunite; B) rounded apatite hosted within ultramafic-rich clastic semi-massive sulfide; C) apatite vein hosted within dolerite. Average chondrite normalised Rare Earth Element (REE) profiles of apatite (D-F): D) ultramafic hosted apatite; E) ore sulfide hosted apatite; F) dolerite associated apatite. Fields show mean and max and minimum ranges. Normalisation values from (Sun and McDonough, 1989).

not carbonatitic in composition and interpreted to be the result of carbonate from a mantle source undergoing Rayleigh fractionation, accounting for the spread in signatures (Fig. 19). The model proposed by Blanks et al. (2020) suggests mantle-derived CO_2 can physically transport sulfide blebs as buoyant compound droplets up into the crust. It may be possible that Munali represents a highly unusual upper crustal expression of such a process, where both sulfide and carbonate have not just remained associated into the upper crust, but have concentrated and formed an ore deposit. However, this association is likely lost in the upper crust as sulfide dissolves and CO_2 decouples, therefore an origin for the carbonate and sulfide as the collection of compound sulfide-CO_2 droplets (Yao et al., 2020) for an upper crustal deposit like Munali seems implausible.

Instead, it has been suggested that wet evaporite-bearing carbonate rocks can be sufficiently melted by mafic intrusives, as observed in IOA (iron-oxide-apatite) deposits that intrude carbonate strata (Bain et al., 2020), where carbonate anataxis was promoted by the low silica content of the mafic melt, alongside abundant volatiles (e.g. CO_2 and chloride salts) which can depress the carbonate eutectic, forming immiscible carbonic melts and brines that can be present late in the system. Thus, given the host rocks at Munali are marbles (and likely evaporite-bearing; Blanks et al., 2022; Evans, 2017), it is perhaps more likely, and supported by C-O isotopes (Figs. 18 and 19) that a component of mantle derived carbonate at Munali has mixed with anatectic derived carbonate, forming carbonate melts that crystallised late into the system, which was then followed by the infiltration of sulfide melts (Blanks et al., 2022), as observed in mine face exposures (Fig. 5B,C and 9A-C).

Carbonate melts derived from marble country rocks have also been proposed at Jinchuan in China, an intrusive complex of a similar age and geotectonic setting to Munali, with Cu-Ni-PGE sulfide mineralisation. At Jinchuan, the interaction of crustally-derived carbonate melts has been proposed to be associated with increased fO_2 that aided saturation of sulfide (Ding et al., 2021; Lehmann et al., 2007); not only forming carbonate rich hybrid rocks, similar to the hybrid rocks of the marginal units of Munali (Fig. 6), but also producing similar carbonate C-O isotopic signatures to Munali (Ding et al., 2021). Other mafic intrusions that show similar evidence for partial melting and assimilation of carbonate-rich country rocks include the Ioko-Dovyren intrusion, Russia (Wenzel et al., 2002) and Nova (Barnes et al., 2020a). At Munali we have clear field evidence for the interaction with crustal carbonate, and the intrusion of late stage carbonate and sulfide melts within the final stages in the evolution of the Munali system (Fig. 9). Consequently, in addition to a mantle derived C component, it appears that the majority of the carbonate at Munali may be crustally derived, yet both may play critical roles in the formation and transportation of magmatic sulfide. The mantle C may suggest the involvement of a carbonatitic-phoscorite component. However, if there is a carbonatite/phoscorite affinity, then the apatite that is also unusually abundant at Munali, and so intimately linked with the carbonate and dunites, should show carbonatitic-phoscorite signatures as well.

10.2. The origin of apatite at Munali

Apatite is a common mineral in many magmatic systems where it usually forms as small (<1 mm) equant to acicular minerals in both silicic and carbonatitic-phoscoritic systems (Webster and Piccoli, 2015),

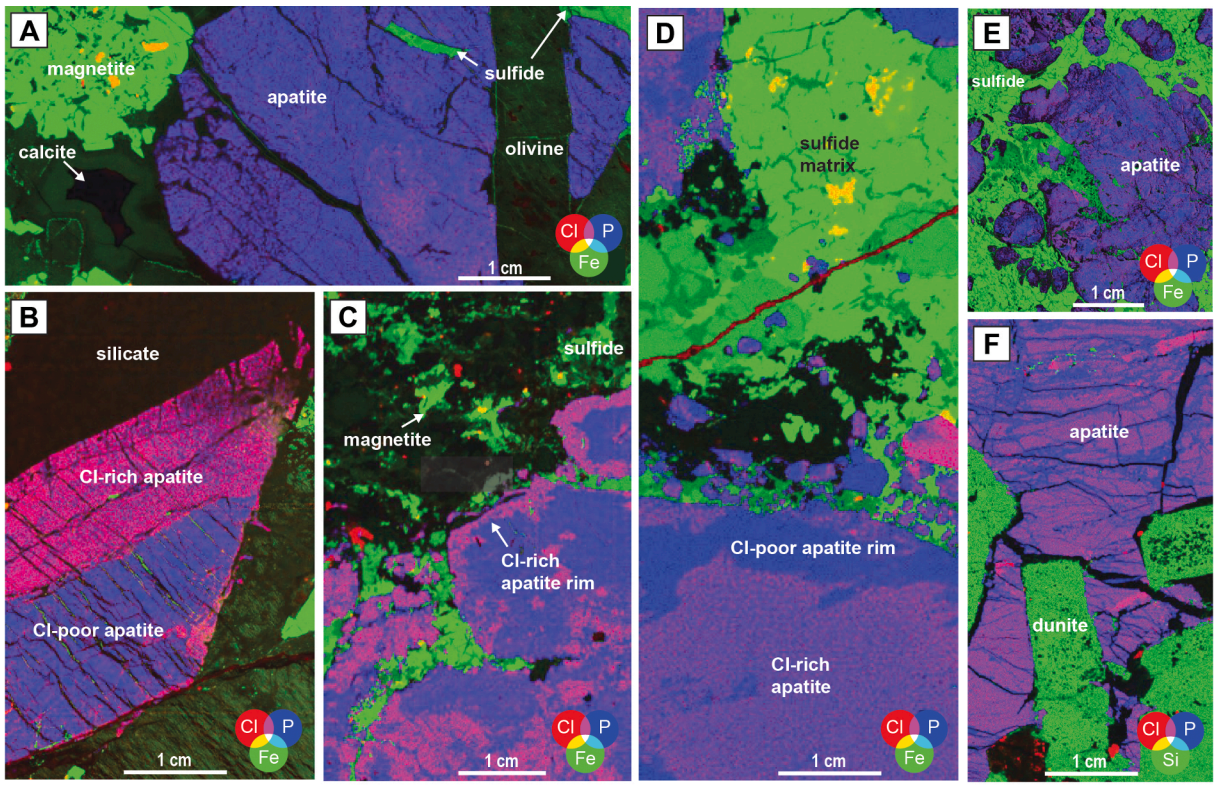

Fig. 16. XRF Tornado™ chemical maps highlighting variable Cl-concentrations within apatite; A) Cl-poor apatite as interstitial phase in dunite, additional host to magnetite, sulfide and calcite; B) Cl-rich and Cl–poor apatite within ultramafic rock; C) Cl-rich rims of apatite within carbonate-magnetite-rich sulfide; D) apatite with Cl-poor rim hosted by sulfide; E) apatite clasts hosted within sulfide; E) apatite associated with ultramafic rocks showing overall Cl-enrichments being Cl-poor apatite along fractures.

but at Munali, can be several centimetres in size (Fig. 8,11,15,16). Apatite has been reported as abundant large crystals in carbonatites (Krasnova et al., 2004); nelsonites (apatite-silicate-magnetite rocks commonly associated with anorthosite massifs; Dymek and Owens, 2001; He et al., 2016); IOCGs (iron-oxide-copper–gold) deposits e.g. Carajás, Brazil (Garcia et al., 2020; Schutesky and de Oliveira, 2020) and Kitumba, Zambia (Milani et al., 2019); IOA deposits e.g. Kiruna, Sweden (Harlov et al., 2002) as well as the El Laco magnetite lava flow in Chile (Mungall et al., 2018). Apatite in mafic–ultramafic rocks is typically present as an accessory component; and (rarely, in highly fractionated mafic layered intrusions) as a primary cumulus phase. Apatite is also becoming increasingly recognised in other sulfide-bearing mafic–ultramafic systems which include Jinchuan (Liu et al., 2021), Marathon deposit of the Coldwell Complex, Canada (Brzozowski et al., 2020; Good et al., 2015), Noril'sk, Siberia (Serova and Spiridonov, 2018; Sluzhenikin et al., 2020) and Nebo-Babel, Australia (Seat et al., 2007), yet the abundance and size at Munali is exceptional.

The isotopic evidence for potential assimilation of carbonate host rocks, and therefore CO_2, would support the probability for the addition of other sedimentary-derived volatiles and halogens (e.g. SO_2 and HCl from evaporites; Heimdal et al., 2019; Iacono-Marziano et al., 2017) during magmatic emplacement. The dominant halogens in apatite can be a useful source and/or fluid discriminant. At Munali, it is mostly Cl, however, in most mafic or other igneous systems F-rich apatite dominates, with Cl-apatite, although present in carbonate-metasomatised mantle xenoliths (Ionov et al., 1996; O'Reilly and Griffin, 2000; Hughes et al., 2017) and layered intrusions (Skaergaard; Namur and Humphreys, 2018 and Kivakka (Barkov and Nikiforov, 2016), are typically thought to partially represent magmatic fractionation or interaction with saline fluids (Doherty et al., 2014; Kusebauch et al., 2015; O'Reilly and Griffin, 2000). The new evidence we show in Fig. 16 shows irregular Cl enrichment in cores, rims, and along cracks in apatite. This attests not to primary Cl-enrichment but more likely due to the interaction of Cl-rich fluids with primary igneous apatite (Kusebauch et al., 2015), which is entirely plausible given the evidence from abundant scapolite schists in the Munali area and scapolite alteration of the gabbroic rocks at Munali, with calcian–marialite compositions (Katongo et al., 2011; Evans, 2017), and the inference of the former presence of evaporite horizons in the host sedimentary rocks (Katongo et al., 2011; Blanks et al., 2022; Evans, 2017).

The nature of the Munali apatite, as very coarse interstitial crystals, is more unusual compared to most ultramafic–mafic rocks, although phoscorites and nelsonites are notable exceptions. Due to their rarity, little geochemical characterisation has been carried out on phoscorites and at present, classification is defined by modal mineral abundance (Krasnova et al., 2004). Using this classification, the ultramafic rocks at Munali, would actually represent an apatite-poor phoscorite that sits towards, and mostly within, the classification as 'magnetite-forsterite' rocks (Fig. 20A). Thus, if the ultramafic rocks are truly phoscorites sensu stricto, they represent the silicate-rich end member of carbonatite magmatism, which would support a scenario whereby the mafic and ultramafic intrusives in the complex are actually not cogenetic, but represent melts from two separate sources.

Trace elements, and in particular the REE concentrations within apatite, are all useful and reliable geochemical indicators into the evolution of a variety of magmatic systems and provide a snapshot of trace element geochemistry of the melt system at time of crystallisation, if present as a cumulus phase (Belousova et al., 2002; Webster and Piccoli, 2015; Mao et al., 2016). The apatite hosted within the ultramafic rocks, associated with dolerite, and within sulfide, all show similar trace element geochemical patterns (Fig. 15D-F), with moderate LREE/HREE ratios and La/Yb_N around 8, with the dolerite-apatite displaying a slightly steeper profile with La/Yb_N of 17.

Fig. 20B-F shows discrimination fields of apatite compositions

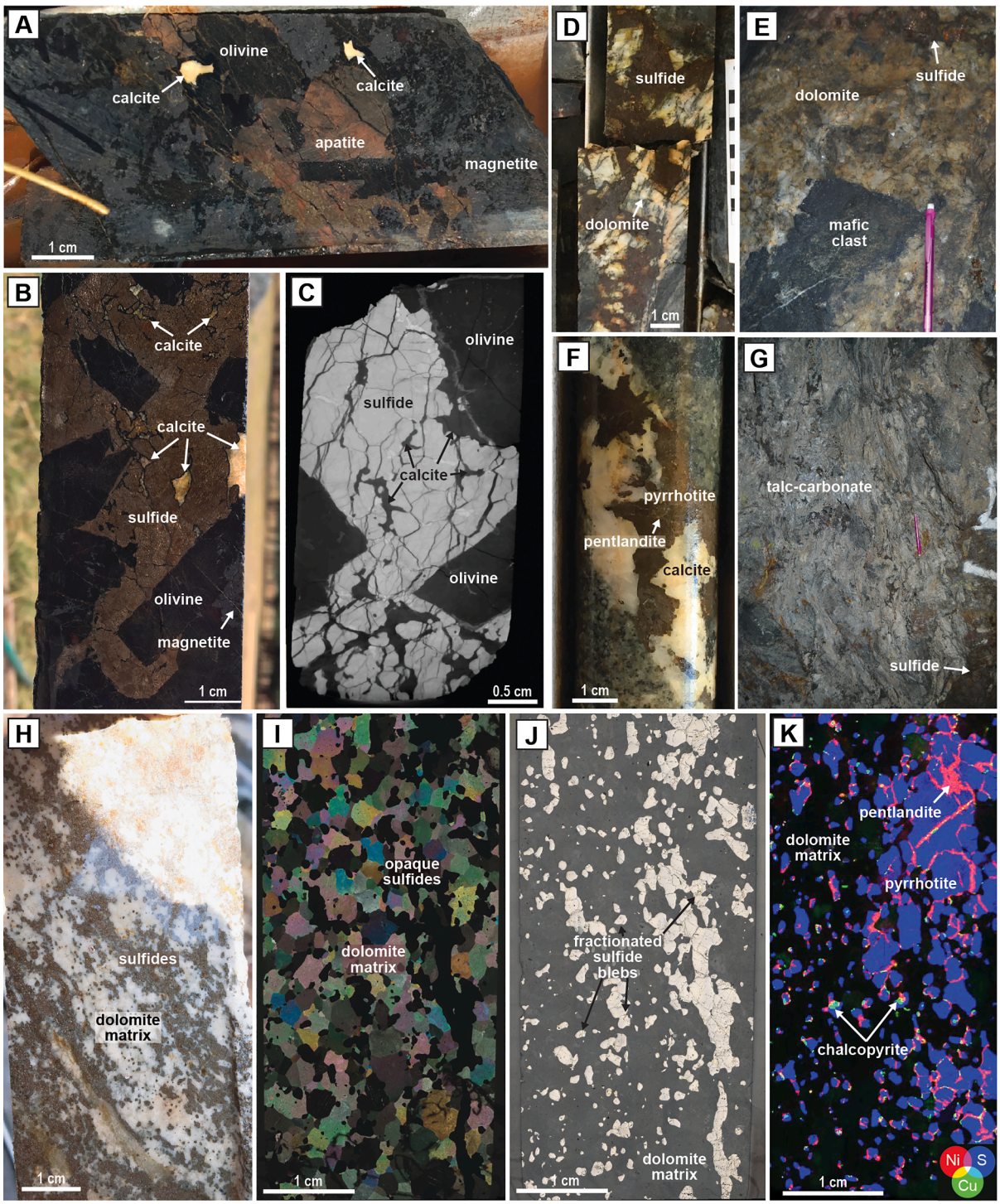

Fig. 17. Carbonate styles of the Munali Intrusive Complex. A) Interstitial calcite hosted within magnetite and apatite-bearing dunite (sample of Fig. 8A); B) interstitial calcite hosted by sulfide with olivine dunite clasts; C) CT scan image of sample in B showing interstitial interconnecting texture of calcite hosted within dunite-bearing sulfide. D) dolomite hosted within sulfide; E) crystalline dolomite with sulfide along the edge of mafic clasts; F) carbonate-sulfide vein in the central gabbro; G) massive talc-carbonate with minor sulfide; H) drillcore sample of sulfide blebs hosted by carbonate matrix; I) transmitted cross-polarised image of sulfide hosted within carbonate matrix with equigranular texture; J) reflected light image of sample shown in I showing sulfide bleb textures; K) XRF Tornado^{TM} chemical map of sample shown in I and J highlighting magmatic sulfide loop textures.

(Belousova et al., 2002; Mao et al., 2016) along with the three apatite styles from Munali. The clustering of the Munali samples reflects their similar trace element geochemistry irrespective of style (Fig. 20D-F). Although the C and O isotopes of the ultramafic rocks at Munali indicate the presence of some primary magmatic carbonate, the Munali apatite do not plot in the carbonatite/phoscorite field in any of the discrimination diagrams shown in Fig. 20. Trace elements of Munali apatite provide no evidence of a phoscoritic origin (Mao et al., 2016; Belousova et al., 2002); phoscorite apatites typically display no Eu anomaly (Fig. 20F, Fig. 21), host Ce anomalies and high REE contents reflecting enrichment of REE in carbonatite magma. Instead apatite at Munali shows characteristics most similar to apatite from a MORB, mafic

Table 1
Summary of analysed $\delta^{13}C$ and $\delta^{18}O$ isotope signatures of carbonates.

Sample	Carbonate	$\delta^{13}C$ VPDB	$\delta^{18}O$ VPDB	$\delta^{18}O$ VSMOW
Munali Complex				
Ultramafic-hosted				
020–302	*calcite*	−4.2	−25.5	4.6
020-302a	*calcite*	−4.0	−25.5	4.6
020-302b	*calcite*	−4.1	−24.9	5.2
Sulfide-interstitial				
020–316	*calcite*	−7.0	−22.1	8.2
020–315	*calcite*	−7.0	−20.0	10.3
020-315b	*calcite*	−6.9	−19.9	10.4
020–318	*calcite*	−6.3	−21.7	8.5
020–320	*calcite*	−6.8	−23.6	6.6
Sulfide-hosted				
U77-01	*dolomite*	−1.7	−18.6	11.8
002–145.7	*dolomite*	−0.1	−18.5	11.8
012-227a	*dolomite*	−0.2	−21.2	9.0
223–382	*dolomite*	−0.8	−18.7	11.6
074–23	*dolomite*	−0.5	−17.9	12.5
091–103	*dolomite*	−0.1	−18.8	11.5
133–139	*dolomite*	0.1	−19.6	10.7
030–84.3	*dolomite*	−1.1	−19.8	10.5
092–70.8	*dolomite*	−0.5	−19.0	11.3
069–107	*dolomite*	−2.3	−19.4	10.9
023–132.5	*dolomite*	−0.2	−19.2	11.2
023–143	*dolomite*	−2.2	−19.2	11.1
032–17	*calcite*	−1.2	−18.4	11.9
U077-57	*calcite*	−3.5	−17.5	12.9
U121-130.2	*dolomite*	−0.2	−17.7	12.7
U121-130.2b	*dolomite*	−0.4	−17.6	12.7
023-143b	*calcite*	−1.1	−21.1	9.2
L820-fw	*calcite*	−1.6	−19.5	10.8
L795-fw	*calcite*	−2.3	−18.5	11.9
012–227	*dolomite*	−0.5	−21.3	9.0
017–255.3	*dolomite*	−1.9	−14.6	15.9
060-304d	*dolomite*	−1.2	−16.4	14.0
074–2.75	*dolomite*	−0.1	−13.5	17.0
105–3	*dolomite*	−2.8	−13.9	16.6
U074-1	*calcite*	−2.6	−14.6	15.8
133–139	*calcite*	1.6	−17.6	12.8
u074-1	*calcite*	−1.6	−24.0	6.1
u70-80	*calcite*	−1.8	−24.2	6.0
u70-80b	*calcite*	−1.6	−24.3	5.9
Talc-carbonate				
017–259	*magnesite*	−2.0	−8.2	22.4
U077-38	*magnesite*	−2.3	−19.7	10.6
012–245	*magnesite*	−0.3	−20.9	9.4
015–213	*magnesite*	−3.4	−18.5	11.8
045–138.5	*magnesite*	−2.8	−15.8	14.6
105–28	*magnesite*	−3.1	−17.6	12.7
023–126	*dolomite*	−0.4	−17.5	12.9
U130-1.5	*dolomite*	−0.5	−18.8	11.5
020–360.2	*magnesite*	−1.5	−15.0	15.5
015–213.5	*magnesite*	−2.4	−15.2	15.3
017–248.5	*dolomite*	−2.6	−16.9	13.5
091–75	*magnesite*	1.5	−25.1	5.0
Munali Hills				
Country rock - marble				
060–125.5 (white)	*calcite*	−0.6	−12.7	17.9
060–125.5 (grey)	*calcite*	1.4	−9.4	21.3
038–176.6	*calcite*	0.7	−10.8	19.7
069–560	calcite	0.4	−13.7	16.8
223–337.5	*calcite*	−3.1	−9.2	21.5
223-354a	*dolomite*	−2.1	−13.4	17.1
223-354b	*dolomite*	−1.8	−14.0	16.5
WP43 (white)	*calcite*	4.7	−6.2	24.5
WP43 (grey)	*calcite*	4.6	−5.8	24.9
WP47b	calcite	−0.3	−9.7	20.9
WP774	*calcite*	5.0	−11.0	19.5
WP775	*calcite*	4.1	−10.9	19.7
WP776	*calcite*	5.2	−9.6	21.0
WP777	*calcite*	5.8	−5.8	24.9
WP778	*calcite*	4.8	−8.2	22.4
WP778-9	*calcite*	−4.3	−6.6	24.1
WP780	*calcite*	4.7	−8.2	22.5
WP781	*calcite*	3.9	−7.7	23.0
WP782	*calcite*	2.8	−14.8	15.7
WP783	*calcite*	4.7	−12.9	17.7
WP784	*calcite*	5.2	−11.8	18.8
WP785	*calcite*	3.7	−8.0	22.7
WP786	*calcite*	3.0	−6.5	24.2
WP787	*calcite*	2.8	−10.7	19.9
WP790	*calcite*	2.6	−11.6	19.0
WP790b	*calcite*	−5.3	−9.3	21.3
Country rock - carbonate-schist				
020–274	*calcite*	2.6	−5.8	25.0
060–189.3	*calcite*	−4.0	−11.3	19.3
223-330a	*calcite*	0.4	−14.9	15.5
223-330b	*calcite*	−0.7	−13.9	16.6
Chibuku intrusion - (sulfide-carbonate veins in gabbro)				
trc-006a	*calcite*	0.2	−17.8	12.6
trc-006a	*calcite*	0.2	−17.9	12.5
trc-006b	*calcite*	0.2	−18.2	12.2
trc-006b	*calcite*	0.2	−17.9	12.4
trc-006c	*calcite*	0.6	−11.4	19.2
trc-006c	*calcite*	0.7	−11.3	19.3
Carbonatite from Keshya, Zambia				
WRTR	calcite	−3.2	-28.6	1.4
Keshya.1	*calcite*	−3.7	−27.6	2.4
Keshya.2	*calcite*	−3.4	−28.6	1.4
TCRK1	*calcite*	−4.1	−25.5	4.6
TCRK2	*calcite*	−5.4	−21.3	8.9
Phoscorite from Kovdor, Russia				
k44721	*calcite*	−2.6	−23.2	7.0
k44721b	*calcite*	−2.6	−23.2	7.0
k44732	*calcite*	−3.4	−23.9	6.3
Phoscorite from Phalaborwa, South Africa				
p23757	*calcite*	−3.0	−22.3	7.9
p74725	*calcite*	−1.7	−15.8	14.6
p74726	*calcite*	−2.5	−21.7	8.5

dolerite or IOA/IOCG system (Fig. 20, Fig. 21). Thus, although apatite and carbonate may be magmatic accessory components to the ultramafic suite at Munali, the apatite data is inconsistent with a carbonatitic/phoscoritic source and therefore an alternative genetic model is required.

10.3. Origin and evolution of the Munali Intrusive Complex

The MIC is comprised of multiple intrusions of mafic and ultramafic magmas emplaced during a relatively short time span (<4 Ma; Holwell et al., 2017), with the mafic portion emplaced prior to the ultramafic units. The unusual mineralogy and geochemistry of the ultramafic rocks remains perplexing, but after ruling out a carbonatitic-phoscoritic origin, our new geochemical data on all the magmatic components of Munali allow us to investigate the magmatic origins of the complex, which do not appear to represent typical host rocks to magmatic Ni-Cu-PGE mineralisation, such as pyroxenites, dunites, or harzburgites.

The mafic igneous rocks of the MIC show distinctly similar flat chondrite-normalised REE profiles (Fig. 14) and MORB-normalised trace element profiles with Th/Yb_N ratios of 0.855, consistent with slightly enriched primitive MORB source. This is supported by the apatite REE data for both mafic and ultramafic rocks which also falls into the MORB field (Fig. 20). Similarities between whole rock profiles suggest all the gabbros and also the wehrlites (Fig. 14) are cogenetic, with only slight variations in REE profiles that can be attributed to different abundance and compositions of trapped liquids of the different mafic magmas (central gabbro, marginal gabbro and dolerite); whereas the dunites show more spread in REE compositions correlating with apatite abundance in the whole rock (Fig. 14). Dunites show depletion in the middle REE, exhibiting a characteristic trough shaped profile controlled by the middle REE more strongly partitioning into apatite over light and heavy REE, and increasing with SiO_2 content of the melt (Prowatke and

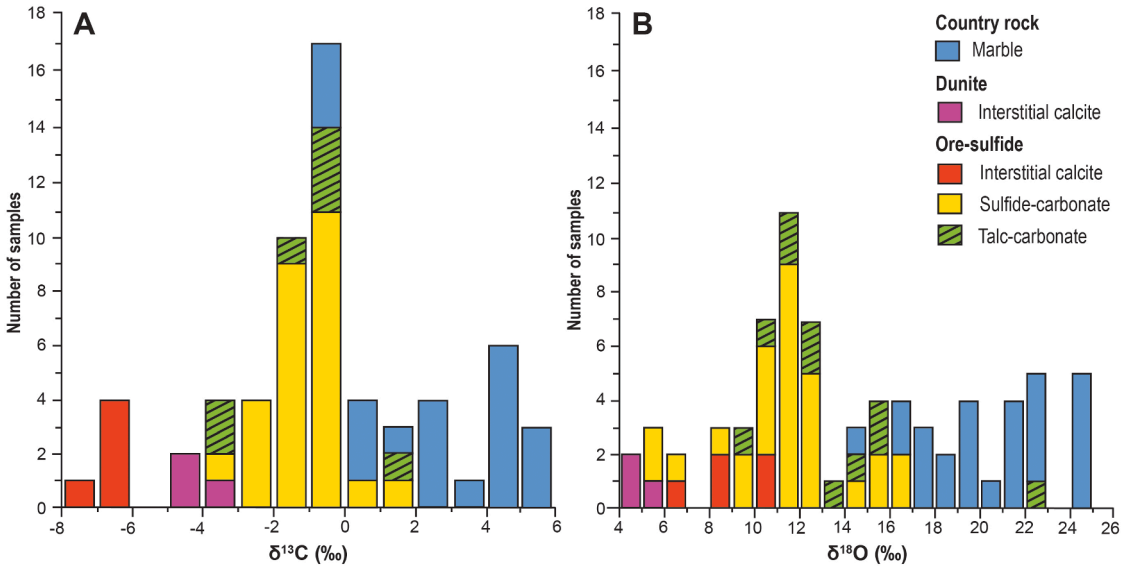

Fig. 18. Isotopic data histogram of carbonate within the Munali Intrusive Complex and country rock marble; A) carbon as ‰ $\delta^{13}C$ relative to VPDB; B) oxygen as ‰ $\delta^{18}O$ relative to VSMOW.

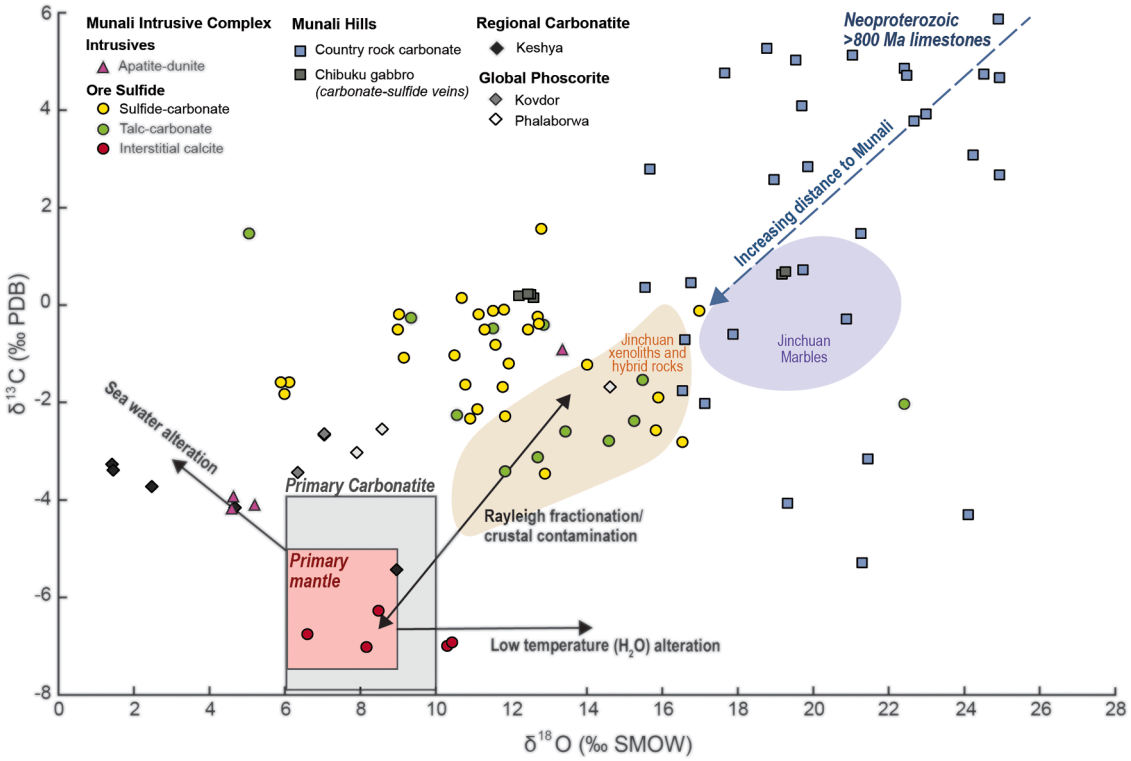

Fig. 19. Carbon and oxygen isotope compositions of carbonates from the different carbonate styles within the Munali Intrusive Complex compared with local country rock marble, carbonate from Keshya (the nearest identified carbonatite) and global phoscorites-carbonatite complexes, Kovdor and Phalaborwa. Fields of primary igneous mantle by Taylor et al. (1967); primary mantle-derived carbonatites by Keller and Hoefs (1995); global carbonatites by Deines (1989) and Jinchuan data fields from Ding et al. (2021).

Klemme, 2006; Watson and Green, 1981). As such, this MREE depletion is representative of the composition of olivine/serpentine within the dunites, whereas the enriched profiles are indicative of the additional presence of apatite (c.f. apatite REE profiles in Fig. 15D-F where bulk rock P_2O_5 is above 1 wt% in Fig. 14C). This suggests that the variability of bulk rock REE in the ultramafic rocks is strongly controlled by modal mineralogy, whereby apatite (plus other phosphates i.e. accessory xenotime) has a disproportionate influence of REE signatures in the ultramafic rocks.

It is worth noting that the apparent similarity between the wehrlite and the mafic rocks in terms of REE (Fig. 14), suggesting that this ultramafic phase may be more related to the mafic rocks. The dunites may well be of a similar origin to the mafic rocks and werhlites, but have been altered, although their differences do raise the possibility they formed from a separate magma. Crustal feeder zones and pathways, such as the Munali Fault, can continuously be a pathway for a range of

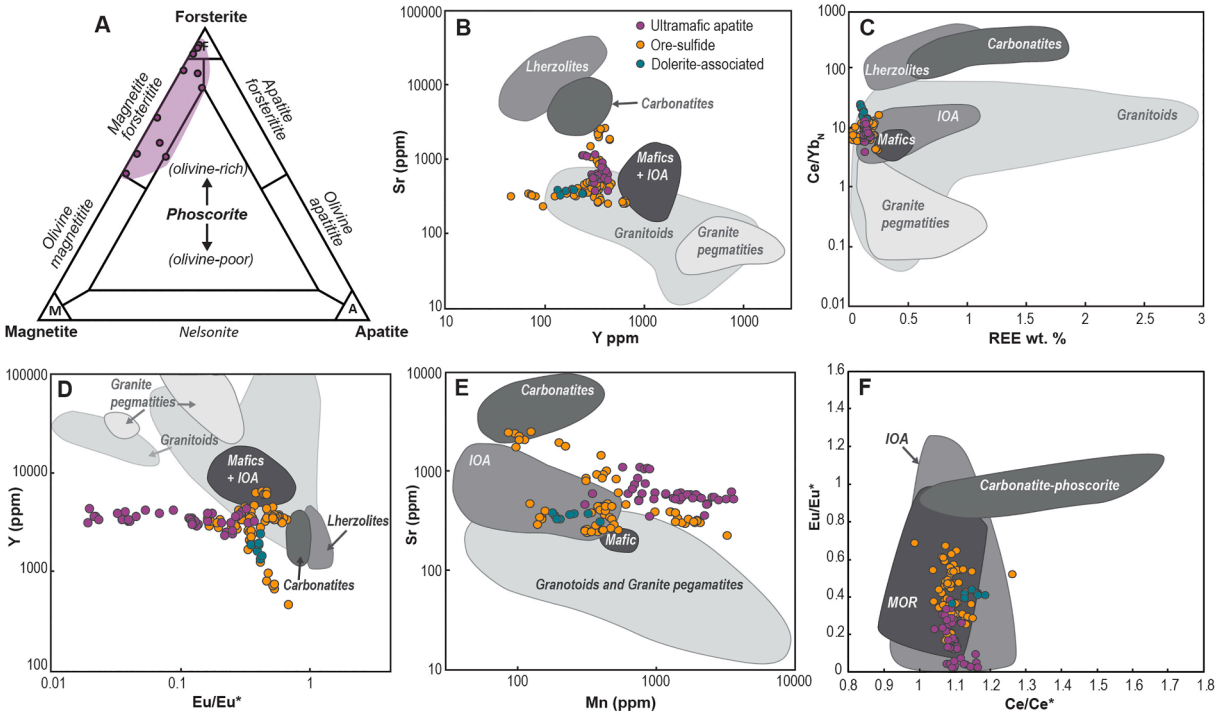

Fig. 20. Apatite discrimination diagrams – IOA = iron-oxide-apatite; MOR = mid ocean ridge. A) Munali ultramafic rocks plotted on phoscorite modal mineralogy classification from Krasnova et al. (2004); B) Y ppm vs Sr ppm; C) REE wt. % vs Ce/Yb$_N$ (chondite normalisation values from McDonough and Sun, 1995); D) Eu/Eu* vs Y ppm; E) Mn ppm vs Sr ppm; F) Ce/Ce* vs Eu/Eu*. (B-E after Belousova et al., 2002 and F after Mao et al., 2016).

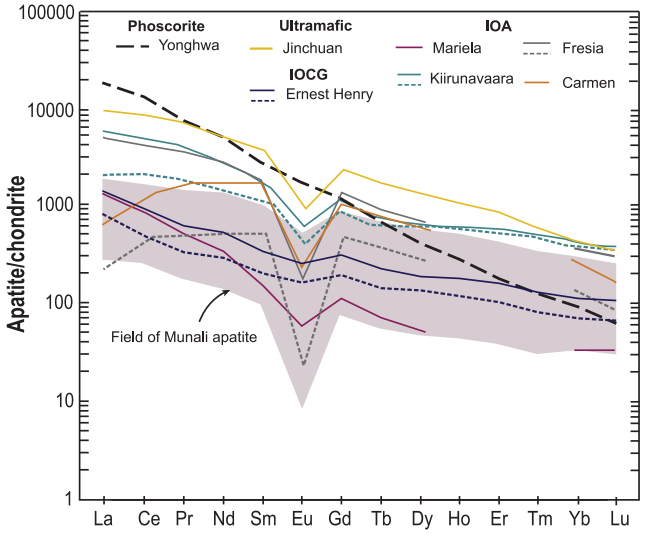

Fig. 21. Field of Munali apatite in comparison to Yonghwa phoscorite apatite (Seo et al., 2016) and IOCG and IOA apatite (dashed line represents altered apatite): IOCG - Ernest Henry, Australia (Cave et al., 2018); mafic–ultramafic apatite – Jinchuan (Liu et al., 2021); IOA – Kiirunavaara, Sweden (Harlov et al., 2002); and IOA – Fresia, Carmen and Mariela, Chile (Palma et al., 2019).

magmas and it is possible that melts from two different sources may have utilised the Munali Fault around the same time. As such, it is not out of the question that mantle melts from different sources could have utilised the same pathways to produce a composite intrusion.

The origin of the dunite, pyroxenite and wehrlite and their relation to the gabbro intrusions is key to elucidating the emplacement history, which our new geochemical data allows us to test. Whilst there is a difference in REE and trace element geochemistry between the wehrlites (more akin to the mafic rocks) and the dunites and apatite-bearing dunites (Fig. 14), their major element geochemistry is comparable (Fig. 13) and all the ultramafic rocks are unusual in that they are very coarse grained and extremely low in Cr. In addition, the abundance of apatite and magnetite in all the ultramafic rocks at Munali are anomalously high, as both are typically present in ultramafic rocks as accessory phases rather than being principal minerals, as they are at Munali. Thus, despite the variations in trace elements of the ultramafic rocks, we suggest they are almost certainly related, and given the similarity in trace element geochemistry between the wehrlite, gabbro and dolerites, plus the very close timing of emplacement (Holwell et al., 2017), the ultramafic rocks may also have the same origin as the earlier mafic magmas.

Whilst some unusual variations in the olivine-rich ultramafic rock chemistry can be ascribed to modal mineralogy, sample heterogeneity or interaction with carbonate and chlorine-bearing fluids, there are some features that are consistent. The ultramafic rocks exhibit high MgO contents due to the abundance of olivine and occasionally clinopyroxene, yet unusually, have exceedingly low Cr contents below 150 ppm (Fig. 13F). Whilst this is consistent with a phoscorite origin, which typically have Cr contents < 100 ppm (Krasnova et al., 2004), phoscorites also have Ni contents in a similar low range. However, sulfide-free (determined from bulk S and Cu values) Munali ultramafic rocks contain between 333 and 784 ppm Ni (Fig. 13H). Therefore, rather than the bulk chemistry supporting a phoscoritic origin, it represents a very Cr-poor apatite-bearing ultramafic rock. High bulk rock Cr is usually a function of the abundance of pyroxene, olivine, or chromite; however, at Munali the Cr content of the ultramafic rocks is below the expected range of > 1000 ppm for typical ultramafic lithologies within magmatic sulfide systems (Liang and Elthon, 1990). With the absence of chromite, magnetite is the sole spinel-oxide phase, not just within the ultramafic rocks but additionally also within the mafic intrusions, and thus may reflect high fO_2 of the magmas.

The apparent absence of Cr within the Munali suite may represent an inherent primary melt feature e.g. from an evolved melt; although it is unlikely an evolved melt would have produced so much olivine.

Alternatively it may be the product of processes that occurred prior to final crystallisation. Early crystallisation of Al-bearing spinel; chromite, or Cr-rich magnetite, would sufficiently deplete concentrations of Cr in the residual melt, resulting in the depleted Cr in the ultramafic rocks, and the absence of chromite and Cr-enriched magnetite. Such scenarios have been suggested in the gabbroic intrusions associated with the Emeishan basalts in China, such as the Honge intrusion that is host to magnetite-rich orebodies, associated with (olivine)-clinopyroxenites and gabbros with up to 10 modal % apatite (Liu et al., 2015), where distinct generations of magnetite show extreme variation in Cr (<1000 ppm and > 10,000 ppm). In these intrusions, interaction of CO_2 from decarbonisation of carbonate-rich sedimentary rocks have been suggested to increase fO_2 and trigger early crystallisation and segregation of Fe-Ti oxides (Ganino et al., 2008). The presence of abundant carbonate at Munali, and interaction with host limestone, attests to a potential role of CO_2 in determining magmatic conditions, and the analogous suite of rocks, including apatite, would support a similar explanation for the lack of Cr at Munali. We therefore propose that the lack of Cr at Munali is a function of early magnetite crystallisation that depleted the ultramafic system of Cr before final crystallisation of the rocks present within the MIC.

The unusual evolving trend with increasing MgO content (Fig. 13) correlates with a decrease in the age of emplacement, whereby the central gabbro is the earliest intrusion having the lowest MgO, and the dunite and wehrlite represent the latest intrusions with the highest MgO content. Interestingly, this trend appears to suggest an overall increase of MgO with time, which is the opposite expected due to fractionation. Given the geochemical and timing constraints, a model whereby the overall magmatic system evolves from a mafic one, to a gradually more ultramafic one, and where a possible geochemical break or divergence comes after the wehrlite and before the dunites, seems the most likely given the evidence we present. Although unusual, intriguingly similar associations of apatite-magnetite bearing ultramafic rocks intruded into earlier mafic rocks have been observed in other magmatic complexes globally, which may be analogous to Munali.

The sulfide-bearing Seiland Complex in Norway (Grant et al., 2016; Larsen et al., 2018) and the Marathon Cu-PGE deposit in the Coldwell Complex, Canada (Good and Crocket, 1994) are both complexes associated with an evolving, increasingly MgO-rich system. The Marathon deposit is host to Pd- and Cu-rich mineralisation attributed to be associated with both hydrothermal and magmatic processes (Good and Crocket, 1994; Good et al., 2015; Brzozowski et al., 2020) emplaced during the beginning of rifting, as Munali was. The complex is host to mafic and ultramafic intrusions comprised of rocks that are highly comparable to those at Munali: poikilitic and pegmatitic gabbro, troctolite and cross cutting sulfide bearing oxide-apatite-olivine clinopyroxenite. In the Marathon rocks, up to 50 modal % Cl-apatite and magnetite are associated with Cr poor (~171 ppm) ultramafic cumulates (average whole-rock P_2O_5 contents of 6 wt%) and similarly represent the youngest phase of the complex, cross-cutting the mafic intrusions and interpreted to be spatially associated with feeder channels to the system (Good et al., 2015). The comparisons to Munali are compelling, although no satisfactory model has yet been proposed for the origin of these rocks at Marathon.

The Sieland Complex, in many ways, shares an even more strikingly similar suite of rocks to Munali, with sequential emplacement of gabbro, olivine gabbro, olivine-clinopyroxenite, wehrlite and dunite, alongside late-stage carbonate melts (Larsen et al., 2018), but in this case, an explanation has been put forward by Grant et al. (2016) to the origin of the sequence. They propose that the rocks reflect metasomatic reactions of younger, hotter, dry, MgO-rich melts emplaced into earlier partially-crystallised gabbro, creating the clinopyroxene and olivine-rich assemblages. The model of Grant et al. (2016) as illustrated in Larsen et al. (2018) involves (1) the initial emplacement of gabbros, followed by (2) hotter (>1400 °C), MgO-rich melts that cause an initial partial melting of clinopyroxene and orthopyroxene in the gabbros forming a 'contact' zone of olivine gabbros. This olivine gabbro then forms a thermochemical barrier between the gabbro and the hot melts which (3) starts to form wehrlitic cumulates. This is then followed by (4) metasomatic reaction by hot MgO melts that replaces the clinopyroxene in the wehrlites, forming a 'replacive' dunite with homogenisation of olivine compositions, and the formation of stratiform magmatic sulfide reefs. In the final stages, aqueous-carbonic alkaline melts infiltrate the unconsolidated dunite, followed by late stage dykes.

Thus, there is a sequence, as at Munali, of (1) early gabbro, followed (2) olivine gabbro, (3) wehrlite and (4) dunites, with late stage infiltration of carbonic melts that is almost identical to that described at Seiland. Indeed, the similar suite of rocks at Sieland, Marathon and Munali may suggest that a similar model can be envisioned for all three complexes. Dunite is the most abundant rock type of the ultramafic suite at Munali, whereas wehrlite and clinopyroxenite are rare, present only as isolated lenses. A replacive origin for the dunite would explain the rarity of pyroxene-rich rocks if most have been effectively replaced, and it would also explain the lack of chilled margins within the intrusive complex. At Munali, evidence of this evolving and replacive sequence can be observed best within limited drill holes where clinopyroxene is abundant, mainly located within the Intrepid prospect (Figs. 2 and 8). Here, ultramafic rocks are spatially associated with gabbro whereby gabbro appears fractured and infilled by a blackish-brown olivine matrix with rare apatite, magnetite and carbonate (Fig. 8G). The relationships shown in Fig. 8 appear to show evidence of later ultramafic melts infiltrating fractures in gabbro, and forming ubiquitously coarse-grained olivine gabbros (Fig. 7), with clinopyroxenite (Fig. 8F), wehrlite (Fig. 8E) and dunite (Fig. 8A-C), consistent with the order of formation of analogous rocks in the Seiland Complex. In addition, the forsterite content of the olivines ($Fo_{85.1}$ to $Fo_{76.1}$; Grant et al., 2016) at Seiland fall within the same range to forsterite content of olivines reported from Munali ($Fo_{83.2}$ to $Fo_{75.2}$; Holwell et al., 2017), and are clearly magmatic. The presence of the otherwise rare olivine-clinopyroxenite and wehrlite, alongside the relative lack of dunites spatially associated with the pyroxene rich rocks at Intrepid, suggests this part of the complex may have been buffered from the late, dunite-forming, infiltrating ultramafic melts as evidenced by the greater abundance of olivine-gabbro at Intrepid.

Given all this evidence, we propose that a similar 'replacive' origin for the olivine-rich ultramafic rocks at Munali as a result of an evolving, progressively more MgO-rich system may be highly likely, which as such, explains their unusual compositions that do not necessarily represent their parental melt composition and does not need to be explained by multiple, distinct magma sources. We suggest that the progressively more MgO melts were formed as extension developed in the Zambezi Belt, initiating low degrees of melting in the mantle source, forming earlier mafic melts which progressively became higher degree partial melts, with correspondingly higher MgO as asthenospheric upwelling during rifting became more pronounced. Such a model that includes progressively hotter melts reacting and replacing earlier gabbroic and then wehrlitic rocks to form pegmatitic dunites via a metasomatic, replacive origin, with the interaction of carbonic fluids (formed from anatexis of carbonate wall rocks by the hotter melts), is consistent with all the data we present: the field relationships and timings, the geochemistry, the rock types and their relative timings, the C-O isotopes of the carbonate, and the apatite chemistry.

Whilst this model of formation for mafic–ultramafic complexes may seem uncommon, the processes of metasomatic replacement and reaction of hot Fe and Mg-rich melts may generally be more widespread, occurring in a number of igneous complexes. For example, a similar unusual suite of ultramafic rocks are the magnesian dunite pipes and apatite-sulfide-bearing IRUPs (Iron-Rich Ultramafic Pegmatites) of the Bushveld Complex, that in contrast to the lower crustal Sieland Complex, are like Munali, emplaced into the upper crust. These IRUPs, although not widely reported, are abundant and present as coarse-grained discordant pipes that crosscut the Upper Critical Zone (Reid and Basson, 2002) and comprise pegmatitic Fe-Ti oxide bearing dunite,

wehrlite, and clinopyroxenite (Scoon and Mitchell, 1994; Scoon and Mitchell, 2004). Although the origin of IRUP bodies is highly debated (e.g. Benson et al., 2020; Cawthorn et al., 2012; Scoon and Mitchell, 1994), these bodies are thought to represent magmatic replacement of earlier-formed cumulates in response to the infiltration of volatile and Fe-rich melts that utilised early-formed fractures and joints, triggering late-stage high temperature metasomatic replacement with conversion of anorthositic and noritic rocks to pegmatitic magnetite-bearing hortonolite-dunite, wehrlite and clinopyroxenite, via the loss of SiO_2 and addition of MgO, FeO and volatiles (Cameron and Desborough, 1964; Reid and Basson, 2002; Scoon and Mitchell, 1994). Therefore, broadly speaking, the ultramafic rocks of the MIC may represent the result of high temperature magmatic and metasomatic processes that are observed to operate in a broad number of settings, that characteristically, produce late-stage, pegmatitic Mg-rich rocks.

10.4. Physical controls and processes to sulfide emplacement and brecciation

The field relationships clearly show that major sulfide emplacement as sheets and breccia-fills with associated carbonate, represents the latest stages in the evolution of the complex, with carbonate preceding sulfide (Fig. 9). In addition, the model presented in Blanks et al (2022) shows how sulfide and carbonate melts were most likely formed elsewhere in the conduit system along the Munali Fault, and were injected/flowed down and along the pre-formed contact between the mafic and ultramafic units in the MIC. The identification of different brecciation styles (Figs. 9 and 10) and understanding on the magmatic emplacement highlights a prominent lithological and structural control on ore emplacement, in contrast to the suggestions of it being chaotic. Similarities in brecciation textures are observed in a range of deposits (Staude et al., 2017; Barnes et al., 2018; Le Vaillant et al., 2020; Barnes et al., 2020a). Sulfide at Munali shows a clear spatial relationship with the ultramafic phases, with the bulk of the sulfide spatially associated with ultramafic rocks (Fig. 4), even when they are not present in abundance, such as the narrow intrusions (<1m) at the Voyager and Intrepid prospects (Fig. 8D), the relationship is persistent.

The association of sulfide with ultramafic rocks is characteristic for many magmatic Ni-Cu-(PGE) deposits, i.e. interstitial and net-textured ores (e.g. Barnes et al., 2017a). Variations in sulfide textures provide key insights into sulfide formation and magmatic processes during the final crystallisation of a magmatic system, whereby interstitial and net-textured sulfide are clearly cogenetic with silicates, indicative of sulfide liquid trapping and infiltration around silicate crystals into pore spaces, yet at Munali this is absent. Instead (semi-)massive sulfide is present as a series of late-stage elongated sheets (SL1-3) and is most abundant and thickest (SL1; 0.5 – 30 m) at the base of the marginal unit, where it accompanied by both soft- and hard-walled brecciation (Fig. 4).

Sulfide hosted 'interstitially' within the ultramafic rocks show an instantaneous decrease in abundance away from the contact with massive sulfide, and the ultramafic rocks are mainly sulfide-free (e.g. Fig. 8A). This spatial association of sulfide within the ultramafic rocks does not suggest the sulfide is directly sourced from the melt that crystallised the olivines. Rather, any sulfide that is trapped within the ultramafic units, as apparent in disseminated blebs and veins, adjacent to the massive and semi-massive sulfide, formed from the percolation of sulfide melt into the ultramafic rock from a source elsewhere in the magmatic conduit system (Blanks et al. 2022). This process caused soft-walled brecciation, with sulfide infiltrating along silicate grain boundaries during a later emplacement event, creating a pseudo-interstitial texture, whereby the ultramafic rocks act as a surrogate, rather than a parental host to sulfide. Fragments and clasts associated with soft-walled brecciation are most commonly olivine and apatite and we interpret them to be refractory fragments derived from ultramafic rocks. The clear observation of olivine and apatite clasts in massive sulfide close to ultramafic intrusions, and similarly mafic clasts spatially associated with mafic rocks, suggests that these clasts were brecciated in-situ and underwent minimal transport, and thus we interpret a relatively passive sulfide infiltration mechanism (e.g. Barnes et al., 2018).

This is supported by evidence from the REE chemistry of apatite hosted by sulfide that show similar profiles to the apatite as part of the ultramafic assemblage (Fig. 15D and E), suggesting that the sulfide-hosted apatite are likely sourced from the ultramafic rock rather than coming in as a separate later phase. The textures of the apatite also support a disaggregation origin showing a range of sub-angular to rounded morphologies (Fig. 4H, 11, 15B and 16E). It is along these brecciated apatite and ultramafic clasts where sulfide droplets appear to wet the edge of the clasts, forming droplets into an immiscible silicate-sulfide melt (Fig. 11). In contrast to the grain-scale soft walled brecciation, hard-walled brecciation is present on a macro scale, where angular mafic fragments and blocks are hosted by sulfide, and suggest a late-stage brecciation and sulfide infiltration after at least partial crystallisation of both the marginal and central gabbro. On this macro scale, the nature of brecciation does not appear to be chaotic, but instead shows favourable orientations and predictability with sulfide veins sets parallel to the main sulfide lenses (dipping ~ 70° SW; parallel to local sedimentary bedding) with narrow sulfide sets orientated perpendicular to this, dipping to the NW (Fig. 4), wherein addition, ultramafic melts as well as sulfide melts seems to have infiltrated a similar orthogonal fracture set in the gabbros (Fig. 8G).

Munali therefore represents a sulfide matrix breccia deposit that is comprised of both fracture filling and sulfide infiltration brecciation, with a structural (fracture set) and lithological (ultramafic) control on the focussing of sulfide ore. This, and the preferential hard-walled brecciation of the mafic rocks over the ultramafic rocks, puts constraints onto timing and emplacement of sulfide infiltration outlined in Fig. 22.

10.5. Post emplacement deformation

Post-magmatic deformation at Munali is shown by a range of ductile structures throughout the area (Figs. 3 and 12). Regionally, Pan-African orogenesis during the Kuunga Orogeny represents a significant compressional event (Goscombe et al., 2020; Sakuwaha et al., 2022), resulting in the present day NW-SE orientation of the western Zambezi Belt, with NE-SW compression resulting in folding of the Zambezi Supracrustal Sequence that has regionally overprinted prior geotectonic events. Southward directed thrusting during this compression has resulted in progressive folding of the country rock sedimentary rocks (Fig. 3) along with the MIC, and is the main contributor for reactivation of the > 15 km long Munali Fault (Fig. 2), interpreted to originally have been a major extensional normal fault, as a high angle reverse fault. This is supported by differences in metamorphic assemblages of metasedimentary rocks, with upthrow of higher pressure metamorphic rocks to the north of the fault.

The identification of sheath folds in the vicinity of the higher metamorphic grade metasedimentary rocks (Fig. 3A), has proven the location of the Munali Fault for the first time in the field, and the likelihood for its reactivation as a reverse fault, situated just 200 m to the north of the MIC. Due to the fault's proximal location to Munali, and the intensity of deformation in the surrounding metasedimentary rocks, it is not surprising that the MIC shows evidence for progressive deformation, with multi-scale deformation causing folding and boudinage of the intrusive rocks (Fig. 12B-D), alongside the high abundance of talc-carbonate (Figs. 12 and 17G) and the occurrence of late-stage cross-cutting fault zones (Fig. 12A). It is likely that the northern margin of the complex underwent more intense deformation than the southern margin, related to movement along the Munali Fault. This may explain the occurrence of sulfide within the Defiant prospect along the northern margin (Fig. 2) as much thinner, potentially sheared out < 1 m lenses, in addition to the successions of marble and gabbro observed within drillcore. The repetition of these units in drillcore may preserve

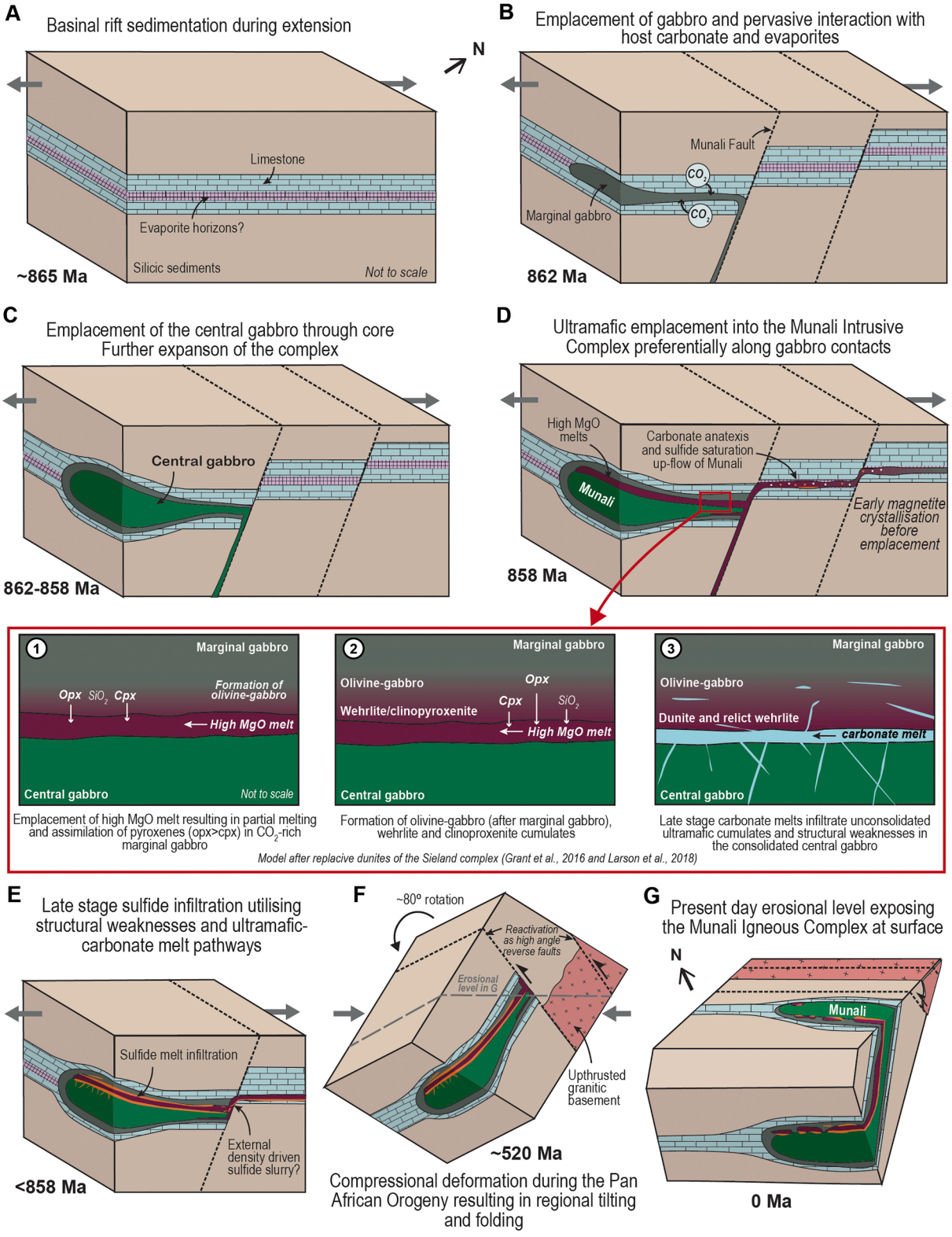

Fig. 22. Relative timing and emplacement of the Munali Intrusive Complex from (A) ~ 865 to (G) present day.

subparallel or secondary fault splays that have caused tectonic shearing and thinning of these units.

The presence of a number of sulfide lenses at Munali (Fig. 4) may be at least in part due to tectonic controls. It is easy to explain the presence of a massive sulfide lens at the footwall boundary of the marginal unit (SL1; Fig. 4), if sulfide was injected along the contact of the ultramafic rocks and central gabbro. This would define the base of the marginal unit, with the central gabbro forming the footwall, if the intrusive complex was emplaced formerly as a sill that has since been rotated to a sub-horizontal orientation (Holwell et al., 2017). Additionally, sulfide utilised other pre-existing structures forming the SL2 and SL3 sulfide bodies, with all sulfide bodies present in similar orientation sets (Fig. 4).

However, the lenticular nature and discontinuity laterally of the thinner sulfide lenses SL2 and SL3, may suggest they have been subjected to post-emplacement deformation and now represent tectonic slivers. Nonetheless, the clear evidence of extensive post-magmatic structural deformation within the orebody contributes to the overall complexity, preservation of the primary features and emplacement mechanism of the MIC.

10.6. Emplacement framework

Utilising our new geochemical and field evidence, along with the S isotopic constraints from Blanks et al (2022) of the various components of the MIC, we are able to advance the emplacement constraints on the relative timings, formation and emplacement of the intrusives and sulfide orebody, plus subsequent deformation, summarised in Fig. 22 and outlined below:

1. Basinal sedimentation during the initiation of rifting and extension along the southern Congo Craton margin between 870 and 862 Ma prior to Munali magmatism (Fig. 22A), including deposition of evaporite-bearing carbonate horizons;
2. Emplacement of low-MgO magmas along the Munali Fault lineament (a translithospheric extensional fault), with marginal gabbro emplaced directly within Zambezi Supracrustal Sequence carbonates, followed by emplacement of the central gabbro causing conduit inflation (Fig. 22B-C);
3. Continued influx of hotter, higher-MgO melts along the Munali lineament, interaction of high-MgO melt with carbonate-rich sediments, promoting carbonate anataxis, sulfide saturation elsewhere in the conduit (Blanks et al. 2022) and triggering crystallisation of Cr-rich magnetite prior to final emplacement (Fig. 22D);
4. Continued influx of high MgO and FeO magmas, causing metasomatic reactions with host marginal gabbro via SiO_2 loss (principally loss of orthopyroxene) forming olivine-gabbros and crystallising pegmatitic apatite-bearing wehrlite and pyroxenites, with continued metasomatism eventually forming replacive dunites (Fig. 22D inset 1-3);
5. Infiltration of mostly crustally-derived carbonate melts (Blanks et al. 2022) along structural weaknesses (Fig. 22D inset 3);
6. Infiltration of a sulfide liquid slurry, sourced from elsewhere in the system (Blanks et al. 2022), utilising structural weaknesses and pathways (previously exploited by carbonate melts) (Fig. 22E). Passive infiltration of sulfide liquid causing brecciation along margins of consolidated ultramafic rocks;
7. Regional compression during the Pan African Orogeny and assembly of Gondwana (resulting in the collision of the Congo and Kalahari Cratons), causing basin inversion, regional folding and reactivation of the Munali Fault as a high-angle reverse fault with variable deformation within the Munali Intrusive Complex (Fig. 22F).

11. Conclusions

The Munali Intrusive Complex represents an unusual, but not unique, dynamic system, preserving the interplay of multiple processes during its evolution. Textural and geochemical relationships imply a sequential emplacement with mafic to ultramafic crystallisation due to the emplacement of magmas with increasing MgO and FeO contents. The hotter and potentially volatile-rich high MgO magmas promoted metasomatic replacement of earlier gabbroic and later pyroxene-rich intrusive bodies, forming exceptional pegmatoidal crystallisation of olivine-rich rocks, and promoting host rock carbonate anatexis. Carbonate within the ores shows intimate relationships with sulfide and micro–macro textures signifying the presence of carbonate melts that are not carbonatitic in origin, with C and O isotopic signatures highlighting the interaction of mantle and predominately sedimentary carbonate from largely crustally derived melts. The emplacement of MORB-like mafic and ultramafic magmas into volatile- and carbonate-rich sediments is proposed to have caused carbonate devolatilisation and anataxis as the main source of the exceptional late-stage carbonate melts, alongside triggering early magnetite crystallisation and depleting the residual magma in Cr. Although host to Ni-(Cu-PGE) sulfide mineralisation, the characteristic carbonate- and apatite-magnetite-rich assemblage is likely to be a function of magmatic processes analogous to those involved in some IOA deposits, where carbonate anatexis has been proposed (e.g. Bain et al. 2020). Sulfide infiltration was the final stage of emplacement within the complex and the absence of primary silicate-sulfide textures, and occurrence of sulfide as a series of metre-scale semi- massive to massive sulfide lenses associated with late-stage brecciation implies the sulfide was not generated in-situ, but introduced to the complex from elsewhere in the system. As such, Munali represents a complex dynamic intrusive system, preserving the final stages from a section of a much larger conduit plumbing system, with only some of the genetic processes preserved in situ.

Declaration of Competing Interest

The authors declare that they have no known competing financial interests or personal relationships that could have appeared to influence the work reported in this paper.

Data availability

Data will be made available on request.

Acknowledgements

The authors would like to thank the staff and management at Mabiza Resources and Consolidated Nickel Mines for facilitating access, sample collection and logistical support at the Munali Nickel Mine, especially Simon Purkiss, Matt Banda and Craig Bailey. Danny Musemeka and Josh Duforest are thanked for their assistance in the field. DB's PhD research was funded by Consolidated Nickel Mines and the University of Leicester. Adam Cox is thanked for assistance in the ICP-MS analysis at the UoL, The manuscript benefited from the constructive reviews by an anonymous reviewer.

Appendix A. Supplementary data

Supplementary data to this article can be found online at https://doi.org/10.1016/j.oregeorev.2022.105109.

References

Bain, W.M., Steele-MacInnis, M., Li, K., Li, L., Mazdab, F.K., Marsh, E.E., 2020. A fundamental role of carbonate–sulfate melts in the formation of iron oxide–apatite deposits. Nat. Geosci. 13, 751–757.

Barkov, A.Y., Nikiforov, A.A., 2016. Compositional Variations of Apatite, Fractionation Trends, and a Pge-bearing Zone in the Kivakka Layered Intrusion, Northern Karelia, Russia. Canad. Mineral. 54, 475–490.

Barnes, S.J., Anderson, J.A.C., Smith, T.R., Bagas, L., 2008. The Mordor Alkaline Igneous Complex, Central Australia: PGE-enriched disseminated sulfide layers in cumulates from a lamprophyric magma. Miner. Deposita 43, 641.

Barnes, S.J., Cruden, A.R., Arndt, N., Saumur, B.M., 2016. The mineral system approach applied to magmatic Ni–Cu–PGE sulphide deposits. Ore Geol. Rev. 76, 296–316.

Barnes, S. J., Taranovic, V., Schoneveld, L. E., Mansur, E. T., Le Vaillant, M., Dare, S., Staude, S., Evans, N. J., and Blanks, D., 2020b, The Occurrence and Origin of Pentlandite-Chalcopyrite-Pyrrhotite Loop Textures in Magmatic Ni-Cu Sulfide Ores: Econom. Geol., v. 115, p. 1777-1798.

Barnes, S.J., Holwell, D.A., Le Vaillant, M., 2017a. Magmatic Sulfide Ore Deposits. Elements v. 13, 89–95.

Barnes, S.J., Le Vaillant, M., Lightfoot, P.C., 2017b. Textural development in sulfide-matrix ore breccias in the Voisey's Bay Ni-Cu-Co deposit, Labrador, Canada. Ore Geol. Rev. 90, 414–438.

Barnes, S.J., Mole, D.R., Hornsey, R., Schoneveld, L.E., 2019. Nickel-Copper Sulfide Mineralization in the Ntaka Hill Ultramafic Complex, Nachingwea Region, Tanzania. Econom. Geol. 114, 1135–1158.

Barnes, S.J., Robertson, J.C., 2019. Time scales and length scales in magma flow pathways and the origin of magmatic Ni–Cu–PGE ore deposits. Geosci. Front. 10, 77–87.
Barnes, S.J., Staude, S., Le Vaillant, M., Piña, R., Lightfoot, P.C., 2018. Sulfide-silicate textures in magmatic Ni-Cu-PGE sulfide ore deposits: Massive, semi-massive and sulfide-matrix breccia ores. Ore Geol. Rev. 101, 629–651.
Barnes, S.J., Taranovic, V., Miller, J.M., Boyce, G., Beresford, S., 2020a. Sulfide Emplacement and Migration in the Nova-Bollinger Ni-Cu-Co Deposit, Albany-Fraser Orogen, Western Australia. Econom. Geol. 115, 1749–1776.
Begg, G.C., Hronsky, J.A.M., Arndt, N.T., Griffin, W.L., O'Reilly, S.Y., Hayward, N., 2010. Lithospheric, Cratonic, and Geodynamic Setting of Ni-Cu-PGE Sulfide Deposits. Econ. Geol. 105, 1057–1070.
Belousova, E.A., Griffin, W.L., O'Reilly, S.Y., Fisher, N.I., 2002. Apatite as an indicator mineral for mineral exploration: trace-element compositions and their relationship to host rock type. J. Geochem. Explor. 76, 45–69.
Benson, E., Connolly, J. A. D., and Boudreau, A. E., 2020, Reply to discussion of 'Crustal fluid contamination in the Bushveld Complex, South Africa: an analogue for subduction zone fluid migration' by Roger Scoon and Andrew Mitchell (2020): Int. Geol. Rev., p. 1-6.
Blanks, D.E., Holwell, D.A., Barnes, S.J., Schoneveld, L.E., Fiorentini, M.L., Baublys, K.A., Mbiri, L., Knott, T.R., 2022. Mobilization and Fractionation of Magmatic Sulfide: Emplacement and Deformation of the Munali Ni-(Cu-Platinum Group Element) Deposit, Zambia. Econom. Geol. https://doi.org/10.5382/econgeo.4906.
Blanks, D.E., Holwell, D.A., Fiorentini, M.L., Moroni, M., Giuliani, A., Tassara, S., González-Jiménez, J.M., Boyce, A.J., Ferrari, E., 2020. Fluxing of mantle carbon as a physical agent for metallogenic fertilization of the crust. Nat. Commun. 11, 4342.
Brzozowski, M. J., Samson, I. M., Gagnon, J. E., Good, D. J., and Linnen, R. L., 2020, Oxide mineralogy and trace element chemistry as an index to magma evolution and Marathon-type mineralization in the Eastern Gabbro of the alkaline Coldwell Complex, Canada: Mineral. Depos.
Bull, S., Selley, D., Broughton, D., Hitzman, M., Cailteux, J., Large, R., McGoldrick, P., 2011. Sequence and carbon isotopic stratigraphy of the Neoproterozoic Roan Group strata of the Zambian copperbelt. Precambr. Res. 190, 70–89.
Cameron, E.N., Desborough, G.A., 1964. Origin of certain magnetite-bearing pegmatites in the eastern part of the Bushveld complex, South Africa. Econom. Geol. 59, 197–225.
Cave, B.W., Lilly, R., Glorie, S., Gillespie, J., 2018. Apatite Geochronology, and Geochemistry of the Ernest Henry Inter-lens: Implications for a Re-Examined Deposit Model. Minerals 8.
Cawthorn, R.G., Ellam, R.M., Ashwal, L.D., Webb, S.J., 2012. A clinopyroxenite intrusion from the Pilanesberg Alkaline Province, South Africa. Precambr. Res. 198–199, 25–36.
Chalice-Mining, 2020, ASX announcement, April: Significant nickel-palladium discovery confirmed at Julimar. https://chalicemining.com/sites/default/files/financial_reports/20200428%20ASX%20Quarterly%20Activities%20Report%20Mar-20%20Final_compressed.pdf.
De Waele, B., Johnson, S.P., Pisarevsky, S.A., 2008. Palaeoproterozoic to Neoproterozoic growth and evolution of the eastern Congo Craton: Its role in the Rodinia puzzle. Precambr. Res. 160, 127–141.
Deines, P., 1989. Stable isotope variations in carbonatites. In: Bell, K. (Ed.), Carbonatites: Genesis and Evolution. Unwin Hyman, London, pp. 301–359.
Demény, A., Ahijado, A., Casillas, R., and Vennemann, T. W., 1998, Crustal contamination and fluid/rock interaction in the carbonatites of Fuerteventura (Canary Islands, Spain): a C, O, H isotope study: Lithos, v. 44, p. 101-115.
Deng, Y.F., Song, X.Y., Chen, L.M., Zhou, T., Pirajno, F., Yuan, F., Xie, W., Zhang, D., 2014. Geochemistry of the Huangshandong Ni–Cu deposit in northwestern China: Implications for the formation of magmatic sulfide mineralization in orogenic belts. Ore Geol. Rev. 56, 181–198.
Ding, X., Ripley, E.M., Underwood, B.S., Meng, Z., Huang, F., 2021. Behavior of Mg and C-O isotopes during mafic magma-carbonate interaction at the Jinchuan Ni-Cu deposit, North China Craton. Chem. Geol. 562, 120044.
Doherty, A.L., Webster, J.D., Goldoff, B.A., Piccoli, P.M., 2014. Partitioning behavior of chlorine and fluorine in felsic melt–fluid(s)–apatite systems at 50MPa and 850–950°C. Chem. Geol. 384, 94–111.
Dymek, R.F., Owens, B.E., 2001. Petrogenesis of Apatite-Rich Rocks (Nelsonites and Oxide-Apatite Gabbronorites) Associated with Massif Anorthosites. Econ. Geol. 96, 797–815.
Evans, D.M., 2011. Geodynamic setting of Neoproterozoic nickel sulphide deposits in eastern Africa. Appl. Earth Sci. 120, 175–186.
Evans, D. M., 2017, Fe-Ni-Cu sulfide-evaporite association at Munali, Zambia: Proceedings of the 14th SGA Biennial Meeting, Québec City, Canada.
Ganino, C., Arndt, N.T., Zhou, M.-F., Gaillard, F., Chauvel, C., 2008. Interaction of magma with sedimentary wall rock and magnetite ore genesis in the Panzhihua mafic intrusion, SW China. Mineral. Depos. 43, 677.
Garcia, V.B., Emilia Schutesky, M., Oliveira, C.G., Whitehouse, M.J., Huhn, S.R.B., Augustin, C.T., 2020. The Neoarchean GT-34 Ni deposit, Carajás mineral Province, Brazil: An atypical IOCG-related Ni sulfide mineralization. Ore Geol. Rev. 127, 103773.
Good, D.J., Crocket, J.H., 1994. Genesis of the Marathon Cu-platinum-group element deposit, Port Coldwell alkalic complex, Ontario; a Midcontinent rift-related magmatic sulfide deposit. Econom. Geol. 89, 131–149.
Good, D.J., Epstein, R., McLean, K., Linnen, R.L., Samson, I.M., 2015. Evolution of the Main Zone at the Marathon Cu-PGE Sulfide Deposit, Midcontinent Rift, Canada: Spatial Relationships in a Magma Conduit Setting. Econ. Geol. 110, 983–1008.
Goscombe, B., Foster, D.A., Gray, D., Wade, B., 2020. Assembly of central Gondwana along the Zambezi Belt: Metamorphic response and basement reactivation during the Kuunga Orogeny. Gondwana Res. 80, 410–465.
Govindaraju, K., 1994. 1994 compilation of working values and sample description for 383 geostandards. Geostandards Newsletter 18, 1–158.
Graham, S.D., Holwell, D.A., McDonald, I., Jenkin, G.R.T., Hill, N.J., Boyce, A.J., Smith, J., Sangster, C., 2017. Magmatic Cu-Ni-PGE-Au sulfide mineralisation in alkaline igneous systems: An example from the Sron Garbh intrusion, Tyndrum, Scotland. Ore Geol. Rev. 80, 961–984.
Grant, T.B., Larsen, R.B., Anker-Rasch, L., Grannes, K.R., Iljina, M., McEnroe, S., Nikolaisen, E., Schanche, M., Øen, E., 2016. Anatomy of a deep crustal volcanic conduit system, The Reinfjord Ultramafic Complex, Seiland Igneous Province, Northern Norway. Lithos 252–253, 200–215.
Hanson, R.E., Wilson, T.J., Wardlaw, M.S., 1988. Deformed batholiths in the Pan-African Zambezi belt, Zambia: Age and implications for regional Proterozoic tectonics. Geology 16, 1134–1137.
Hanson, R.E., Wilson, T.J., Munyanyiwa, H., 1994. Geologic evolution of the neoproterozoic Zambezi orogenic belt in Zambia. J. Afr. Earth Sc. 18, 135–150.
Harlov, D.E., Andersson, U.B., Förster, H.-J., Nyström, J.O., Dulski, P., Broman, C., 2002. Apatite–monazite relations in the Kiirunavaara magnetite–apatite ore, northern Sweden. Chem. Geol. 191, 47–72.
He, H.L., Yu, S.Y., Song, X.Y., Du, Z.S., Dai, Z.H., Zhou, T., Xie, W., 2016. Origin of nelsonite and Fe–Ti oxides ore of the Damiao anorthosite complex, NE China: Evidence from trace element geochemistry of apatite, plagioclase, magnetite and ilmenite. Ore Geol. Rev. 79, 367–381.
Heimdal, T. H., Callegaro, S., Svensen, H. H., Jones, M. T., Pereira, E., and Planke, S., 2019, Evidence for magma–evaporite interactions during the emplacement of the Central Atlantic Magmatic Province (CAMP) in Brazil: Earth and Planetary Science Letters, v. 506, p. 476-492.
Holwell, D.A., Blanks, D.E., 2021. Emplacement of magmatic Cu-Au-Te(-Ni-PGE) sulfide blebs in alkaline mafic rocks of the Mordor Complex, Northern Territory, Australia. Mineral. Depos. 56, 789–803.
Holwell, D.A., Mitchell, C.L., Howe, G.A., Evans, D.M., Ward, L.A., Friedman, R., 2017. The Munali Ni sulfide deposit, southern Zambia: A multi-stage, mafic-ultramafic, magmatic sulfide-magnetite-apatite-carbonate megabreccia. Ore Geol. Rev. 90, 553–575.
Horstmann, U.E., Verwoerd, W.J., 1997. Carbon and oxygen isotope variations in southern African carbonatites. J. Afr. Earth Sc. 25, 115–136.
Hughes, H.S.R., McDonald, I., Loocke, M., Butler, I.B., Upton, B.G.J., Faithfull, J.W., 2017. Paradoxical co-existing base metal sulphides in the mantle: The multi-event record preserved in Loch Roag peridotite xenoliths, North Atlantic Craton. Lithos 276, 103–121.
Iacono-Marziano, G., Ferraina, C., Gaillard, F., Di Carlo, I., Arndt, N.T., 2017. Assimilation of sulfate and carbonaceous rocks: Experimental study, thermodynamic modeling and application to the Noril'sk-Talnakh region (Russia). Ore Geol. Rev. 90, 399–413.
Imai, N., Terashima, S., Itoh, S., Ando, A., 1995. 1994 compilation of analytical data for minor and trace elements in seventeen GSJ geochemical reference samples, "Igneous Rock Series". Geostandards Newsletter 19, 135–213.
Imai, N., Terashima, S., Itoh, S., Ando, A., 1996. 1996 compilation of analytical data on nine GSJ geochemical reference samples, "Sedimentary Rock Series". Geostandards Newsletter 20, 165–216.
Imai, N., Terashima, S., Itoh, S., Ando, A., 1999. 1998 compilation of analytical data for five GSJ geochemical reference samples: the "Instrumental Analysis Series". Geostandards Newsletter 23, 223–250.
Ionov, D.A., O'Reilly, S.Y., Genshaft, Y.S., Kopylova, M.G., 1996. Carbonate-bearing mantle peridotite xenoliths from Spitsbergen: phase relationships, mineral compositions and trace-element residence. Contrib. Miner. Petrol. 125, 375–392.
Járóka, T., Seifert, T., Pfänder, J.A., Staude, S., Seibel, H.V.L., Krause, J., Bauer, M.E., 2019. Geology, sulfide mineralogy and petrogenesis of the Angstberg Ni-Cu-(PGE) sulfide mineralization (Lausitz Block, Bohemian Massif, Germany): A potential Ni-Cu exploration target in Central Europe? Ore Geol. Rev. 110, 102924.
Jesus, A.P., Mateus, A., Benoit, M., Tassinari, C.G.G., Bento dos Santos, T., 2020. The timing of sulfide segregation in a Variscan synorogenic gabbroic layered intrusion (Beja, Portugal): Implications for Ni-Cu-PGE exploration in orogenic settings. Ore Geol. Rev. 126, 103767.
Johnson, S.P., Rivers, T., De Waele, B., 2005. A review of the Mesoproterozoic to early Palaeozoic magmatic and tectonothermal history of south–central Africa: implications for Rodinia and Gondwana. J. Geol. Soc. 162, 433–450.
Johnson, S.P., De Waele, B., Evans, D., Banda, W., Tembo, F., Milton, J.A., Tani, K., 2007. Geochronology of the Zambezi Supracrustal Sequence, Southern Zambia: A Record of Neoproterozoic Divergent Processes along the Southern Margin of the Congo Craton. J. Geol. 115, 355–374.
Jones, A.P., Genge, M., Carmody, L., 2013. Carbonate Melts and Carbonatites. Rev. Mineral. Geochem. v. 75, 289–322.
Katongo, C., Koller, F., Kloetzli, U., Koeberl, C., Tembo, F., Waele, B.D., 2004. Petrography, geochemistry, and geochronology of granitoid rocks in the Neoproterozoic-Paleozoic Lufilian-Zambezi belt, Zambia: Implications for tectonic setting and regional correlation. J. Afr. Earth Sc. 40, 219–244.
Katongo, C., Koller, F., Ntaflos, T., Koeberl, C., Tembo, F., 2011. Occurrence and Origin of Scapolite in the Neoproterozoic Lufilian-Zambezi Belt, Zambia: Evidence/Role of Brine-Rich Fluid Infiltration During Regional Metamorphism: Dordrecht. Springer, Netherlands, Dordrecht, pp. 449–473.
Keller, J., Hoefs, J., 1995. Stable Isotope Characteristics of Recent Natrocarbonatites from Oldoinyo Lengai. In: Bell, K., Keller, J. (Eds.), Carbonatite Volcanism: Oldoinyo

Lengai and the Petrogenesis of NatroCarbonatites: Berlin. Heidelberg, Springer, Berlin Heidelberg, pp. 113–123.
Key, R.M., Liyungu, A.K., Njamu, F.M., Somwe, V., Banda, J., Mosley, P.N., Armstrong, R. A., 2001. The western arm of the Lufilian Arc in NW Zambia and its potential for copper mineralization. J. Afr. Earth Sc. 33, 503–528.
Krasnova, N.I., Petrov, T.G., Balaganskaya, E.G., Garcia, D., Moutte, J., Zaitsev, A.N., Wall, F., Wall, F., and Zaitsev, A.N., 2004, Introduction to phoscorites: occurrence, composition, nomenclature and petrogenesis, Phoscorites and carbonatites from mantle to mine: the key example of the Kola alkaline province, Mineralogical Society of Great Britain and Ireland.
Kusebauch, C., John, T., Whitehouse, M.J., Engvik, A.K., 2015. Apatite as probe for the halogen composition of metamorphic fluids (Bamble Sector, SE Norway). Contrib. Miner. Petrol. 170, 34.
Larsen, R.B., Grant, T., Sørensen, B.E., Tegner, C., McEnroe, S., Pastore, Z., Fichler, C., Nikolaisen, E., Grannes, K.R., Church, N., ter Maat, G.W., Michels, A., 2018. Portrait of a giant deep-seated magmatic conduit system: The Seiland Igneous Province. Lithos v. 296–299, 600–622.
Le Vaillant, M., Barnes, S.J., Mole, D.R., Fiorentini, M.L., Laflamme, C., Denyszyn, S.W., Austin, J., Patterson, B., Godel, B., Hicks, J., Mao, Y.-J., Neaud, A., 2020. Multidisciplinary study of a complex magmatic system: The Savannah Ni-Cu-Co Camp, Western Australia. Ore Geol. Rev. 117, 103292.
Legend, 2020, Legend Mininig limted - 2019 Annual Report.
Lehmann, J.R.M., Arndt, N., Windley, B., Zhou, M.F., Wang, C.Y., Harris, C., 2007. Field Relationships and Geochemical Constraints on the Emplacement of the Jinchuan Intrusion and its Ni-Cu-PGE Sulfide Deposit, Gansu, China. Econom. Geol. 102, 75–94.
Lesher, C.M., 2017. Roles of xenomelts, xenoliths, xenocrysts, xenovolatiles, residues, and skarns in the genesis, transport, and localization of magmatic Fe-Ni-Cu-PGE sulfides and chromite. Ore Geol. Rev. 90, 465–484.
Li, Z.X., Bogdanova, S.V., Collins, A.S., Davidson, A., De Waele, B., Ernst, R.E., Fitzsimons, I.C.W., Fuck, R.A., Gladkochub, D.P., Jacobs, J., Karlstrom, K.E., Lu, S., Natapov, L.M., Pease, V., Pisarevsky, S.A., Thrane, K., Vernikovsky, V., 2008. Assembly, configuration, and break-up history of Rodinia: A synthesis. Precambr. Res. 160, 179–210.
Liang, Y., Elthon, D., 1990. Evidence from chromium abundances in mantle rocks for extraction of picrite and komatiite melts. Nature 343, 551–553.
Liu, P.P., Zhou, M.F., Chen, W.T., Gao, J.F., Huang, X.W., 2015. In-situ LA-ICP-MS trace elemental analyses of magnetite: Fe–Ti–(V) oxide-bearing mafic–ultramafic layered intrusions of the Emeishan Large Igneous Province, SW China. Ore Geol. Rev. 65, 853–871.
Mao, M., Rukhlov, A.S., Rowins, S.M., Spence, J., Coogan, L.A., 2016. Apatite Trace Element Compositions: A Robust New Tool for Mineral Exploration*. Econ. Geol. v. 111, 1187–1222.
McDonough, W.F., Sun, S.S., 1995. The composition of the Earth. Chem. Geol. 120, 223–253.
Merdith, A.S., Collins, A.S., Williams, S.E., Pisarevsky, S., Foden, J.D., Archibald, D.B., Blades, M.L., Alessio, B.L., Armistead, S., Plavsa, D., Clark, C., Müller, R.D., 2017. A full-plate global reconstruction of the Neoproterozoic. Gondwana Res. 50, 84–134.
Milani, L., Lehmann, J., Naydenov, K.V., Saalmann, K., Nex, P.A.M., Kinnaird, J.A., Friedman, I.S., Woolrych, T., Selley, D., 2019. Geology and mineralization of the Cu-rich Mumbwa district, a potential IOCG-type system at the eastern margin of the Pan-African Hook batholith, Zambia. J. Afr. Earth Sc. 158, 103513.
Mungall, J. E., Long, K., Brenan, J. M., Smythe, D., and Naslund, H. R., 2018, Immiscible shoshonitic and Fe-P-oxide melts preserved in unconsolidated tephra at El Laco volcano, Chile: Geology, v. 46, p. 255-258.
Namur, O., Humphreys, M.C.S., 2018. Trace Element Constraints on the Differentiation and Crystal Mush Solidification in the Skaergaard Intrusion, Greenland. J. Petrol. 59, 387–418.
O'Reilly, S.Y., Griffin, W.L., 2000. Apatite in the mantle: implications for metasomatic processes and high heat production in Phanerozoic mantle. Lithos 53, 217–232.
Palma, G., Barra, F., Reich, M., Valencia, V., Simon, A.C., Vervoort, J., Leisen, M., Romero, R., 2019. Halogens, trace element concentrations, and Sr-Nd isotopes in apatite from iron oxide-apatite (IOA) deposits in the Chilean iron belt: Evidence for magmatic and hydrothermal stages of mineralization. Geochim. Cosmochim. Acta 247, 515–540.
Paton, C., Hellstrom, J., Paul, B., Woodhead, J., Hergt, J., 2011. Iolite: Freeware for the visualisation and processing of mass spectrometric data. J. Anal. At. Spectrom. 26, 2508–2518.
Piña, R., Lunar, R., Ortega, L., Gervilla, F., Alapieti, T., Martínez, C., 2006. Petrology and Geochemistry of Mafic-Ultramafic Fragments from the Aguablanca Ni-Cu Ore Breccia, Southwest Spain. Econom. Geol. 101, 865–881.
Piña, R., Romeo, I., Ortega, L., Lunar, R., Capote, R., Gervilla, F., Tejero, R., Quesada, C., 2010. Origin and emplacement of the Aguablanca magmatic Ni-Cu-(PGE) sulfide deposit, SW Iberia: A multidisciplinary approach. GSA Bullet. 122, 915–925.
Prowatke, S., Klemme, S., 2006. Trace element partitioning between apatite and silicate melts. Geochim. Cosmochim. Acta v. 70, 4513–4527.
Reid, D.L., Basson, I.J., 2002. Iron-rich ultramafic pegmatite replacement bodies within the Upper Critical Zone, Rustenberg Layered Suite, Northam Platinum Mine, South Africa. Mineral. Mag. 66, 895–914.
Rudashevsky, N. S., Kretser, Y. L., Rudashevsky, V. N., Sukharzhevskaya, E. S., Wall, F., and Zaitsev, A. N., 2004, A review and comparison of PGE, noble-metal and sulphide mineralization in phoscorites and carbonatites from Kovdor and Phalaborwa, Phoscorites and carbonatites from mantle to mine: the key example of the Kola alkaline province, Mineralogical Society of Great Britain and Ireland, p. 0.
Sakuwaha, K.G., Tsunogae, T., Banda, P., Changasha, C., Sikazwe, O.N., Tsutsumi, Y., 2022. Neoproterozoic thermal events and crustal growth in the Zambezi Belt, Zambia: New insights from geothermobarometry, monazite dating, and detrital zircon geochronology of metapelites. Lithos 424. https://doi.org/10.1016/j.lithos.2022.106762.
Schutesky, M.E., de Oliveira, C.G., 2020. From the roots to the roof: An integrated model for the Neoarchean Carajás IOCG System, Brazil. Ore Geol. Rev. 127, 103833.
Scoon, R.N., Mitchell, A.A., 1994. Discordant Iron-Rich Ultramafic Pegmatites in the Bushveld Complex and their Relationship to Iron-Rich Intercumulus and Residual Liquids. J. Petrol. 35, 881–917.
Scoon, R.N., Mitchell, A.A., 2004. Petrogenesis of discordant magnesian dunite pipes from the central sector of the Eastern Bushveld Complex with emphasis on the Winnaarshoek pipe and disruption of the Merensky reef. Econ. Geol. 99, 517–541.
Seat, Z., Beresford, S.W., Grguric, B.A., Waugh, R.S., Hronsky, J.M.A., Gee, M.A.M., Groves, D.I., Mathison, C.I., 2007. Architecture and emplacement of the Nebo-Babel gabbronorite-hosted magmatic Ni–Cu–PGE sulphide deposit, West Musgrave, Western Australia. Mineral. Depos. 42, 551.
Seo, J., Choi, S.G., Park, J.W., Whattam, S., Kim, D.W., Ryu, I.C., Oh, C.W., 2016. Geochemical and mineralogical characteristics of the Yonghwa phoscorite–carbonatite complex, South Korea, and genetic implications. Lithos 262, 606–619.
Serova, A.A., Spiridonov, E.M., 2018. Three Types of Apatite in Norilsk Sulfide Ores. Geochem. Int. 56, 474–483.
Sluzhenikin, S.F., Yudovskaya, M.A., Barnes, S.J., Abramova, V.D., Le Vaillant, M., Petrenko, D.B., Grigor'eva, A.V., Brovchenko, V.D., 2020. Low-Sulfide Platinum Group Element Ores of the Norilsk-Talnakh Camp. Econ. Geol. v. 115, 1267–1303.
Smith, A.G., 1963. The geology of the country around Mazabuka and Kafue; explanation of degree sheets 1527, SE quarter and 1528 SW quarter, v. Report of the Geological Survey Department of Zambia, Lusaka.
Staude, S., Barnes, S.J., Le Vaillant, M., 2017. Thermomechanical erosion of ore-hosting embayments beneath komatiite lava channels: Textural evidence from Kambalda, Western Australia. Ore Geol. Rev. 90, 446–464.
Sun, S.S., McDonough, W.F., 1989. Chemical and isotopic systematics of oceanic basalts: implications for mantle composition and processes. Geol. Soc., London, Specl. Publicat. 42, 313.
Taylor, H.P., Frechen, J., Degens, E.T., 1967. Oxygen and carbon isotope studies of carbonatites from the Laacher See District, West Germany and the Alnö District, Sweden. Geochim. Cosmochim. Acta 31, 407–430.
Watson, E.B., Green, T.H., 1981. Apatite/liquid partition coefficients for the rare earth elements and strontium. Earth Planet. Sci. Lett. 56, 405–421.
Webster, J.D., Piccoli, P.M., 2015. Magmatic Apatite: A Powerful, Yet Deceptive, Mineral. Elements 11, 177–182.
Wenzel, T., Baumgartner, L.P., Brügmann, G.E., Konnikov, E.G., Kislov, E.V., 2002. Partial Melting and Assimilation of Dolomitic Xenoliths by Mafic Magma: the Ioko-Dovyren Intrusion (North Baikal Region, Russia). J. Petrol. 43, 2049–2074.
Wilson, N.C., MacRae, C.M., 2005. An Automated Hybrid Clustering Technique Applied to Spectral Data Sets. Microsc. Microanal. 11, 434–435.
Yao, Z., Mungall, J.E., Qin, K., 2020. A Preliminary Model for the Migration of Sulfide Droplets in a Magmatic Conduit and the Significance of Volatiles. J. Petrol. 60, 2281–2316.
Zaitsev, A., Bell, K., 1995. Sr and Nd isotope data of apatite, calcite and dolomite as indicators of source, and the relationships of phoscorites and carbonatites from the Kovdor massif, Kola peninsula, Russia. Contribut. Mineral. Petrol. 121, 324–335.